

Modeling Great Salt Lake water levels and salinities to capture current adaptive management actions

Diana Dunn ^{a,*}, Brian Crookston ^{a,*} , Som Dutta ^b, Bethany Neilson ^a

^a Utah Water Research Laboratory, Dept. of Civil and Env. Engineering, Utah State Univ., 8200 Old Main Hill, Logan, UT 84322-8200, USA

^b Dept. Mechanical and Aerospace Engineering, Utah State University, 8200 Old Main Hill, Logan, UT 84322-8200, USA



ARTICLE INFO

Keywords:

Mass Balance Modeling
Salinity
Applied Hydrology
Adaptive Management
Flow Modeling

ABSTRACT

Study region: The Great Salt Lake (located in Utah, USA) is the largest saltwater lake in the western hemisphere.

Study focus: The Great Salt Lake is a hypersaline, closed basin lake with an east-west rockfill railroad causeway dividing the lake into north and south arms. Recent record low lake levels, increased salinity and water elevation gradients between the two arms have threatened critical ecologic and economic productivity. In response, recent management efforts have focused on a newly constructed submerged berm within a causeway breach, completed December 2016, that has been altered to control bidirectional flow exchange between the higher salinity north arm and the south arm, which receives all freshwater inflows. In this study, a new 1D analytical model of breach exchange flows has been incorporated into a new open-source multi-layer mass balance model of the Great Salt Lake to predict lake levels and salinity.

New hydrological insights for the region: The applied model considers newly combined and curated salinity data from various entities along with relevant hydrologic data and a sensitivity of groundwater contributions. Water level results validated the model formulation and necessary assumptions, with predictions generally within the range of data uncertainty. Further, salinity predictions in the south arm fell within the 90 % confidence intervals. Through model application, the efficacy of the new submerged berm as an adaptive management tool was confirmed, along with the need for additional lake monitoring.

1. Introduction

Since the onset of the Anthropocene, aquatic ecosystems have experienced significant loss of habitat and biodiversity from land conversion and fragmentation, industrialization, infrastructure development, resource extraction, and waste production (Otto, 2018). Terminal saline lakes have been among the most affected; many have experienced desiccation due to agricultural and urban water development within their watersheds (Williams, 1996; Wurtsbaugh et al. 2017) that has stressed or destroyed the unique, diverse biota that they sustain (Hassani et al., 2020). For example, the Aral Sea in Kazakhstan has lost 90 % of its volume (Banks et al., 2022), Lake Urmia in Iran has been reduced by 90 % (AghaKouchak et al., 2015), and Owens Lake in California, USA was completely lost in 1913 before making a recent reappearance due to management actions (Borlina et al., 2017).

The Great Salt Lake (GSL) in Utah, USA is one of the world's largest and most ecologically and economically productive saline lakes.

* Corresponding authors.

E-mail addresses: diana.dunn@usu.edu (D. Dunn), brian.crookston@usu.edu (B. Crookston).

Its biodiverse food web and wetlands (Belovsky et al., 2011) support breeding and migration for millions of water and shorebirds, and it is a critical link in the Pacific Flyway between North and South America (Donnelly et al., 2020). Brine shrimp cyst harvests are used as a food source by global commercial aquaculture operations (Wurtsbaugh, 2014). Minerals are also extracted from the hypersaline brine, supplying various salt-containing products, potassium for fertilizer, and 14% of the world's magnesium, among others (Bioeconomics, 2012). These activities generate approximately 6500 jobs and contribute \$1.9 billion USD (adjusted for inflation) annually to Utah's economy (Bioeconomics, 2012).

Many endeavors have been undertaken to capitalize on GSL resources, which has caused the lake to become highly modified. Notably, in 1959, an east-west rockfill railroad causeway was constructed that segregated the lake into north and south arms (Marden et al., 2020; Fig. 1). All freshwater inflows enter the south arm of the GSL. Segregating the lake altered its spatial and temporal water patterns (Brown et al., 2023) and caused the south arm to develop a higher water surface elevation and significantly lower salinity compared to the north. It also caused the south arm to experience periods of density stratification where a less dense upper brine layer (UBL) forms above a more dense deep brine layer (DBL). This is in part due to high-density north arm water entering the less dense south arm through openings in the causeway (Naftz, 2017). GSL's natural hydrologic balance has also been altered by significant upstream water withdrawals for agricultural and municipal use (Null and Wurtsbaugh, 2020). Since 2000, these water diversions, compounded by a period of prolonged drought (Williams et al., 2020), have triggered a significant decline in annual average lake level and record high salt concentrations (GSL Strike Team, 2023). If the GSL continues on this trajectory, economic activities will suffer

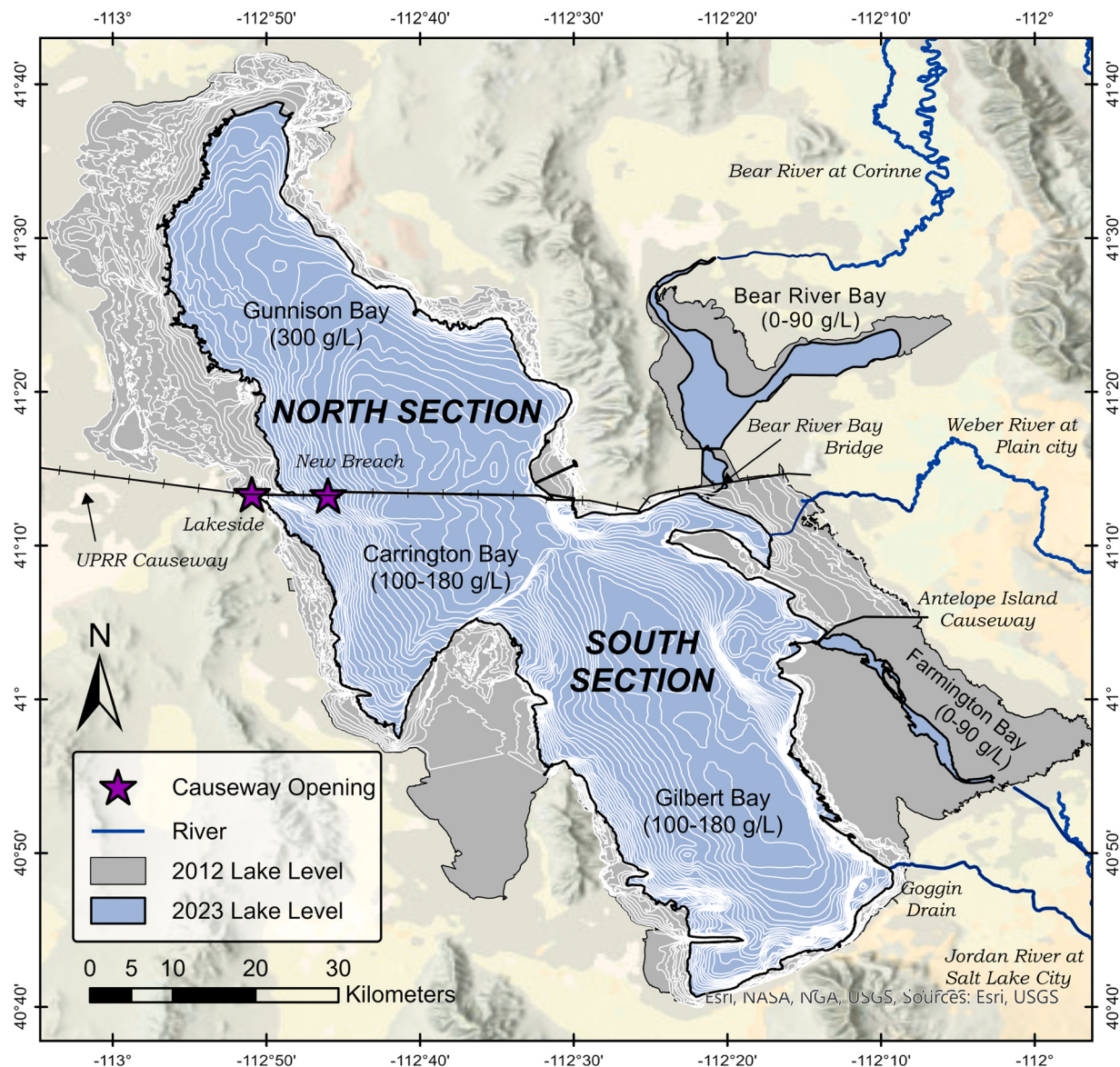


Fig. 1. The Great Salt Lake and its bays, tributaries, and key features.

millions of dollars in damage (ECONorthwest and Martin and Nicholson Environmental Consultants, 2019) with projected long-lasting harm to the ecological communities (Barnes and Wurtsbaugh, 2015; Lindsay et al., 2019; Perry et al., 2019).

Efforts to minimize recent GSL desiccation have focused on adaptively managing south arm lake levels and salinity. Construction of a new bridge and opening in the causeway, the New Breach, was completed in December 2016. The New Breach experiences bidirectional flow exchange where water flows south to north (SN), due to the higher south arm water elevation, while simultaneously water flows north to south (NS) due to the concentration gradient. A submerged berm at the New Breach has been raised multiple times since construction to control this bidirectional flow exchange, facilitating adaptation to changing hydroclimatic conditions. Utilizing the submerged berm as an adaptive management tool is best informed by a detailed understanding of the hydrology and hydrodynamics of the lake, including the interactions between lake water surface elevation, evaporation, and salinity. These are driven by snowmelt, stream flows, climate shifts, and cycling of water and salt between the arms. Prior work has sought to disentangle these complex relationships by quantifying, chronicling, and characterizing changes in south arm dissolved salt mass (Brown et al., 2023; Merck and Tarboton, 2023; Yang et al., 2020). However, they did not quantify rates of change in lake water surface elevations or salt mass and more did they address the influences of fluctuating water levels on salinity.

Previous GSL model studies have targeted different aspects of the lake to meet various management objectives (Jewell, 2021; White et al., 2015; 2019; Loving et al., 2000; Waddell and Fields, 1977; Wold et al., 1996). White et al. (2015) used a single layer mass balance model to inform design of the New Breach in the causeway and the potential effect on south arm salinity. Their work incorporated the USGS' GSL Fortran Model of the bidirectional flow exchange through the old box culverts as documented in Holley and Waddell (1976), Wold et al. (1996) and Loving et al. (2000). These simulations estimated south arm salinity response to various bridge geometries, but did not segregate the south arm into an UBL and DBL. The Great Salt Lake Integrated Model (GSLIM) was developed by Jacobs Engineering in 2017 to predict lake water surface elevation and salinity in response to changes within the watershed by integrating river, wetland, and lake modules. The GSLIM code is inaccessible to technical stakeholders because of the use of proprietary software which creates limited flexibility for adaptation to changing lake conditions, research, and management needs. Further, it does not use all publicly available data pertaining to salinity and includes the old box culvert prediction method to estimate the bidirectional flow exchange at the New Breach. To improve New Breach exchange flow predictions, a computational fluid dynamics model of the New Breach was developed by Rasmussen et al. (2021) in addition to a series of machine learning based models (Larsen, 2024) formulated using historical hydroclimate data (Dunn et al., 2025; Dutta et al., 2024).

Given the limitations of existing GSL models and newly developed causeway flow prediction methods, there is a clear need to inform lake adaptive management efforts via a new open source, process based, stratified mass balance model that more accurately predicts lake levels, salinities, and exchange flows. This model should include all available hydrologic data, encompass current key water and salt mass fluxes, and incorporate New Breach exchange flow rating curves as a function of submerged berm elevation. Also, an open-source model could more easily be updated with new datasets, developments and management strategies. Therefore, the Utah State University Mass Balance Model (USU-MBM) was developed to predict salt concentrations and lake water surface elevations for the north and south arms of the GSL while capturing complex bidirectional exchanges at the causeway and vertical mixing dynamics within the stratified south arm. All available salinity data types collected by diverse stakeholders were compiled and used in both calibration and validation to ensure robust model performance. Accurate prediction of lake water surface elevation and salinity allowed for scenario generation and illustrated the model's capabilities for evaluating recent and future adaptive management strategies while highlighting additional monitoring needs.

2. Materials and methodology

2.1. Study area

The GSL experiences an arid climate with high evaporation rates. Precipitation falls primarily in the form of snow during the winter months, followed by substantial spring runoff (Baxter and Butler, 2020). Lake volume is understood to be most sensitive to the balance between river inflows and evaporation (Mohammed and Tarboton, 2012). Typically, lake water surface elevations decrease from July to October when temperatures are high, the climate is dry, and evaporative volumes exceed river inflows. From November to June, inflow volumes are larger than evaporative volumes due to snowfall and spring snowmelt (White et al., 2015). GSL water surface elevation also varies at an interdecadal scale triggered by periods of drought and flood (Wang et al., 2010).

Inflows to the lake also include direct precipitation (about 30 %) and groundwater (estimated to be 3 %). Groundwater contributions to the lake are not directly measured but have been estimated to be $0.17 \text{ km}^3/\text{yr}$ for the south arm and $0.34 \text{ km}^3/\text{yr}$ for the north arm. Groundwater salinity is near that of river inflows (Zamora and Inkenbrandt, 2024); however, the effects of seasonality on groundwater contributions are unclear. River tributaries (see Fig. 1) contribute about 58 % of total inflows; these include the Bear River (BR) (39 % of known, total streamflow to the lake (Null and Wurtsbaugh, 2020), the Weber River (WR) (10 % of total streamflow), and the Jordan River (JR) (18 % of total streamflow) (Utah Department of Natural Resources, 2022). The JR enters the lake through wetland complexes, to Farmington Bay (FB) and the Goggin Drain (GD). The BR and WR also flow through wetlands before entering the Bear River Bay (BR Bay) and the south arm, respectively. Wurtsbaugh et al. (2017) estimated that these inflows have been depleted by approximately 39 % since 1847, which has lowered the lake water surface by about 3.4 m (a 64 % reduction in volume). 63 % of water diversions are for agriculture, 11 % by cities, 13 % by solar ponds, and 13 % are attributed to other uses (Null and Wurtsbaugh, 2020). Additionally, mineral extraction companies routinely pump water from the north and south arms to evaporation ponds on either side of BR Bay and on the southwest corner of Gilbert Bay (Merck and Tarboton, 2023).

Salinity and nutrient dynamics across the entire lake are heterogenous due to the rockfill railroad causeway. North of the causeway

(Gunnison Bay) the lake water surface elevation is commonly about 0.3–0.6 m lower than that of the south arm. It is also reddish in hue and near saturation with respect to salt (330 g/L). The south arm (Carrington Bay, Gilbert Bay) is a blueish hue with salt concentrations fluctuating between 100 g/L and 180 g/L due to seasons and water year conditions (Wurtsbaugh, 2014; Fig. 1). BR Bay and FB waters are more dilute, generally less than 90 g/L. During periods of stratification, the south arm DBL has a salt concentration around 200 g/L (Merck and Tarboton, 2023). Naftz et al. (2014) documented movement of north arm water between Carrington Bay and Gilbert Bay as a high-density current during infrequent high northerly wind events. Such conditions trigger unidirectional NS flow through openings in the causeway, thus establishing or maintaining the DBL in the south arm (Naftz et al., 2011). Fluctuations in DBL elevation are influenced by extreme wind events that are believed to induce mechanical mixing through the water column; however, full dissipation of the DBL has only been observed when the causeway openings were closed (Yang et al., 2020; Wurtsbaugh and Jones, 2012). South arm mass loading also occurs from river tributaries; however, causeway exchange flows have been assumed to be the main driver of salt mass change since 2010. More recently, Jewell (2021) has considered hypersaline north arm brine seepage across the entire causeway length as another contributor to the DBL; however, additional research is needed to more fully understand seepage through the causeway.

The two arms of the GSL have experienced various levels of connectivity throughout the history of the causeway. Initially, two box culverts provided limited water and salt mass exchange between the arms (Gwynn and Sturm, 1987). The Lakeside Breach was added in 1984 to counteract high south arm lake elevations and flooding of nearby communities. This opening has a relatively high bottom invert elevation and therefore does not effectively connect north and south arms. For example, in the early 2000s when lake levels dropped significantly due to drought conditions, little to no flow was exchanged via the Lakeside Breach. Meanwhile, the original box culverts deteriorated and sank into the lakebed, and by 2013 the two lake arms experienced no documented exchange flows (White et al., 2015). In response, a 55 m wide bridge, the aforementioned New Breach, was opened in December 2016 to reconnect both arms of the lake. The New Breach includes a submerged rock berm that can be raised or lowered (placing or excavating materials) to control bidirectional flow exchange that is driven by the density and water surface elevation differences between the north and south arms (Rasmussen et al., 2021). In 2022 the berm was first modified, raised to an elevation of 1276.2 m to limit increasing salinity levels in the south arm, thus lessening salt mass loading from the north. Despite this raise, the south arm of the lake reached a record low water surface elevation (WSE) and record high salinity. In response, the berm was raised further to an elevation of 1277.7 m that was above the south arm WSE, maximizing dilution during the 2023 spring runoff and allowing UBL salinity to decrease to 125 g/L prior to summer 2023. Recently, Dunn et al. (2025) compiled comprehensive daily hydrologic time series throughout the south arm UBL and DBL using new salinity conversion methods to showcase the key drivers of GSL south arm salinity patterns due to recent New Breach berm managements strategies.

2.2. Model formulation

To address the GSL modeling needs, a mass balance approach was taken to simulate lake elevations and salinities in both the north and south arms, considering all known freshwater contributions, losses, exchange flows through the New Breach, and exchanges between the DBL and UBL in the south arm (see Fig. 2). An overview of the model formulation and method sequence, including objective, input data, and calibration, corroboration, sensitivity, and scenarios is provided in the [Supplemental Information](#) (Fig. S1).

Salt concentration (C), equivalent to salinity (S), is dependent on water volume (V) and total dissolved salt mass (M), both of which vary over time in the GSL. Therefore, model formulation incorporated both V and M balances. Because current adaptive management of the GSL utilizes the New Breach and its submerged berm, the period of analysis for the USU-MBM focused on July 2017 until October 2023. This period corresponds to the start of stable DBL conditions after the New Breach was opened to about 5 years later when the

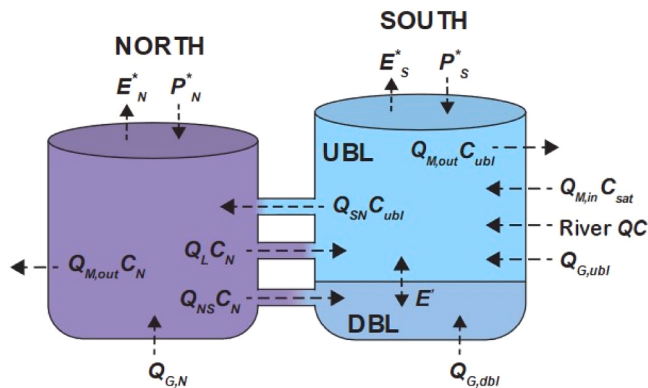


Fig. 2. Conceptual model diagram including water and volume fluxes where River Q includes surface water inflows from the Bear River, Weber River, Goggin Drain, and Farmington Bay, River C is concentration of the River Q , E^* is evaporation, P^* is precipitation, Q_G is groundwater contribution, $Q_{m,out}$ is withdrawal for mineral extraction activities (separate for the north arm and the south arm), $Q_{m,in}$ is return flow from mineral extraction activities, Q_{SN} is south to north New Breach flow, Q_{NS} is north to south New Breach flow, Q_L is flow through Lakeside Breach, C_N is north arm concentration, C_{UBL} is concentration of UBL and E' is mass transfer due to diffusion across the DBL/UBL interface.

submerged berm was raised to completely restrict exchange flows. The simulation period was broken into a calibration period (July 2017 to December 2021) and a validation period (January 2022 to October 2023). Selection of the model time step was informed by available GSL hydrologic data (Dunn et al., 2025) and a sensitivity to averaging data on daily, weekly, and monthly scales. A daily time step was selected because it balanced the uncertainty associated with monthly data, averaging hourly forcing data, and was computationally efficient (computation time for the USU-MBM over the entire 5-year simulation period was about 4 min on a low-power desktop computer).

2.2.1. Mass balance equations

The GSL was divided into two control volumes to represent the north and south arms (Fig. 2). There is inconsistent salinity data for BR Bay and FB, little is known about additional salt and water volume contributions within these areas, and these two bays tend to act independently from the rest of the lake due to freshwater inflows (Dunn et al., 2025). This led to flow and mass contributions being tracked through BR Bay bridge and the FB bridge to estimate inflows to the south arm control volume that included only Carrington Bay and Gilbert Bay (Fig. 1). The south arm control volume was further segregated into two vertical layers with corresponding volumes, the UBL and DBL, to represent documented periodic density stratification. Other commonly applied lake stratification methods were explored, as summarized in [Supplemental Information S4](#), but did not accurately predict DBL elevation compared to the approach documented herein.

The north arm control volume and both south arm control volumes were treated as three completely mixed zones where influxes of water V and M were instantaneously mixed, causing vertical and horizontal homogeneity within each layer. This assumption was made based upon the analysis of limited historical data by Merck and Tarboton (2023), who concluded spatial and vertical homogeneity in both south arm layers and the entire north arm.

In this model, water is supplied to the lake via precipitation as a volume per day (P^*), surface water discharge from the Bear River (Q_{BR}), the Weber River (Q_{WR}), Goggin Drain (Q_{GD}), and Farmington Bay (Q_{FB}), groundwater inflow to the north ($Q_{G,N}$), to the UBL ($Q_{G,ubl}$), and to the DBL ($Q_{G,dbl}$), and return flows from mineral extraction activities ($Q_{M,in}$) (Fig. 2). Lake V is lost to evaporation (E^*) and water pumped out of the GSL for mineral extraction ($Q_{M,out}$) (Fig. 2). Water is exchanged between control volumes via flows through Lakeside Breach (Q_L) and bidirectional flows through the New Breach (Q_{NS} , Q_{SN}). Mineral extraction companies pump water out of both lake arms, thus $Q_{M,out}$ was tracked separately for the north arm and the south arm. UBL V fluxes included Q_{BR} , Q_{WR} , Q_{FB} , Q_{GD} , P^* , E^* , $Q_{G,ubl}$, $Q_{M,out}$, $Q_{M,in}$, Q_{SN} and Q_L , assuming all Q into the lake was fully mixed into the UBL and that the mineral companies pumped brine from the UBL and north arm. Jewell (2021), Yang et al. (2020), and Wurtsbaugh and Jones (2012) analyzed drivers of DBL formation and determined that the DBL forms primarily due to Q_{NS} , thus DBL V fluxes included Q_{NS} . The approximation of $Q_{G,dbl}$ was also included, as described in [Section 2.2.2](#) (Fig. 2). Given these assumptions and V fluxes, the water budget equations for the south arm UBL ($V_{S,ubl}$), south arm DBL ($V_{S,dbl}$) and the north arm (V_N) were:

$$\frac{dV}{dt}_{S,ubl} = Q_L - Q_{SN} + Q_{BR} + Q_{WR} + Q_{FB} + Q_{GD} - Q_{M,out} + Q_{M,in} + P_S^* + Q_{G,ubl} - E_S^* \quad (1)$$

$$\frac{dV}{dt}_{S,dbl} = Q_{NS} + Q_{G,dbl} \quad (2)$$

$$\frac{dV}{dt}_N = Q_{SN} - Q_{NS} - Q_L - Q_{M,out} + P_N^* - E_N^* + Q_{G,N} \quad (3)$$

where Q_{BR} , Q_{WR} , Q_{GD} , Q_{FB} = discharge from GSL tributaries [m^3/day], Q_L = discharge from Lakeside Breach [m^3/day], Q_{NS} = north-to-south discharge through the New Breach [m^3/day], Q_{SN} = south-to-north discharge through the New Breach [m^3/day], $Q_{M,out}$ = withdrawal from mineral extraction activities [m^3/day] (separate for each arm of the lake), $Q_{M,in}$ = return flow to the south arm from mineral extraction activities [m^3/day], P^* = precipitation [m^3/day], E^* = evaporation [m^3/day], and $Q_{G,ubl}$, $Q_{G,dbl}$, $Q_{G,N}$ = groundwater discharge to each control volume [m^3/day]. The explicit Euler method with upwind differencing scheme was used to solve the governing water balance equations (Chapra, 1997; Hoffman, 2001).

Both M and V are exchanged between the UBL and DBL in the south arm due to turbulent diffusion and wind induced turbulent mixing. To represent the latter in the USU-MBM formulation, a wind mixing algorithm ([Eqs. 4–6](#)) was applied to supplement mass transfer due to turbulent diffusion, as high GSL brine density precludes conventional methods. This mixing algorithm incorporates a V threshold to quantify exchange between the DBL and UBL. Based upon limited historical DBL depth observations and insights from USGS, V_{dbl} is, on average, about 9 % of total south arm volume (V_S) where $V_S = V_{ubl} + V_{dbl}$. If $V_{dbl,i+1} > 0.09 \times V_{S,i+1}$, a portion of $V_{dbl,i+1}$ with a concentration equal to the concentration at the beginning of the time step, $C_{dbl,i}$, is mixed into the UBL to maintain this observed threshold. C_i is then updated prior to quantifying M fluxes:

$$V^* = V_{dbl,i+1} - 0.09 \times V_{S,i+1} \quad (4)$$

$$C_{ubl,i}^* = \frac{V_{ubl,i} C_{ubl,i} + V^* C_{dbl,i}}{V_{ubl,i} + V^*} \quad (5)$$

$$C_{dbl,i}^* = \frac{V_{dbl,i} C_{dbl,i} - V^* C_{ubl,i}}{V_{dbl,i} - V^*} \quad (6)$$

where C is in [kg/m³] and V^* is the difference between interim DBL volume and the DBL volume threshold [m³]. M is also exchanged across the UBL/DBL interface due to turbulent diffusion and was represented using a bulk diffusion coefficient as presented within Chapra (1997). Adopting these water budget equations and assuming a completely mixed system, salt mass balances for the south arm UBL, south arm DBL, and the north arm were:

$$\frac{d(VC)}{dt}_{S,ubl} = Q_L C_{N,i} + Q_{BR} C_{BR} + Q_{WR} C_{WR} + Q_{FB} C_{FB} + Q_{GD} C_{GD} - Q_{SN} C_{ubl,i}^* - Q_{M,out} C_{ubl,i}^* \\ + Q_{M,in} C_{sat} + Q_{G,ubl} C_{G,ubl} + E \left(C_{dbl,i}^* - C_{ubl,i}^* \right) \quad (7)$$

$$\frac{d(VC)}{dt}_{S dbl} = Q_{NS} C_{N,i} + Q_{G,dbl} C_{G,dbl} + E \left(C_{ubl,i}^* - C_{dbl,i}^* \right) \quad (8)$$

$$\frac{d(VC)}{dt}_N = Q_{SN} C_{ubl,i}^* + Q_{G,N} C_{G,N} - Q_{NS} C_{N,i} - Q_L C_{N,i} - Q_{M,out} C_{N,i} \quad (9)$$

where C_{BR} , C_{WR} , C_{FB} , C_{GD} = salt concentration of GSL tributaries [kg/m³], $C_{G,ubl}$, $C_{G,dbl}$, $C_{G,N}$ = salt concentration of Q_G flowing to each control volume, $C_{N,i}$ = salt concentration of the north arm at time step i , $C_{ubl,i}$ = salt concentration of the UBL at time step i , $C_{dbl,i}$ = salt concentration of the DBL at time step i [kg/m³], C_{sat} = saturated salt concentration of water at 20 °C [kg/m³], and E = turbulent diffusion coefficient [m³/d]. Merck and Tarboton (2023) found that 25 % of total V pumped from the lake for mineral extraction was returned to the south arm at halite concentration, thus C_{sat} was assumed to be constant with a value of 275 g/L. Following the completely mixed assumption, C of the brine removed from the north arm along with Q_L and Q_{NS} were assumed to be equal to C_N , while C of the brine removed from the UBL and Q_{SN} were assumed to equal C_{ubl} . If UBL/DBL C equalized at the end of a model time step, the DBL was mixed completely into the UBL and DBL growth was allowed until the V threshold was met again. For periods where $V_{S, dbl}$ is small during DBL formation (less than 10,000 m³), the model sets $\frac{d(VC)}{dt}_{S, dbl}$ equal to 0 to avoid model instability prior to full DBL formation.

Two lake processes have been observed at the GSL but are not monitored and thus not accounted for in the USU-MBM: 1) seepage through the causeway (Jewell, 2021) and 2) salt crystal deposition/re-entrainment at the lakebed and lake shores. Jewell (2021) found that seepage along the causeway contributed to DBL formation using limited data gathered from 2008 to 2015. Furthermore, the causeway is routinely (often weekly) modified by the Union Pacific Railroad by adding rock and fill material that may locally alter seepage rates, introducing high uncertainty in any seepage estimates and corresponding salt transfer. Thus, this aspect of the system was not included in the model formulation. Jagniecki et al. (2021) observed salt precipitation from the water column in the north arm during winter months when the water temperature (T) decreased and re-dissolution of salt from the north lakebed due to wave action when water T increased. Although this may potentially be a nonnegligible source of M , specific methods to describe these complex dynamics at the GSL have not yet been developed.

2.2.2. Mass balance term approximations

Precipitation and Evaporation: Daily volumes of precipitation for each arm of the lake were estimated by:

$$P^* = P_d \times A \quad (10)$$

where P^* = precipitation volume, unique for each arm [m³/d], P_d = precipitation depth [m/d] and A = surface area [m²] that is a function of WSE which changes with time. A is dependent on lake V which is calculated for each arm at each timestep based on the U.S. Geological Survey (USGS) high resolution relationship between A and V for each bay as a function of WSE (Root, 2023). For this study, south arm A and V were calculated using these tables by summing values for all portions of the lake considered by the model (i.e., Carrington Bay and Gilbert Bay).

The same method was employed to calculate volume of E at the lake's surface:

$$E^* = E_d \times \%E \times A \quad (11)$$

where E^* = evaporative volume unique for each arm [m³/d], E_d = evaporative depth [m/d], and $\%E$ = percent reduction in E_d , discussed in Section 2.4. E_d was calculated using (Mohammed and Tarboton, 2012):

$$E_d = \frac{\Delta' R_n}{\gamma + \Delta' \lambda_v \rho} + \frac{\gamma}{\gamma + \Delta'} K_E v_w (e_s(T_a) \beta(T_a, C) - e_a(T_d)) \quad (12)$$

where Δ' = saturated vapor pressure gradient for a saline surface [kPa/°C], γ = psychrometric constant [kPa/°C], R_n = net energy available at the water surface [MJ/m² × day], λ_v = latent heat of evaporation [MJ/kg], ρ is in [kg/m³], K_E = bulk latent heat transfer coefficient approximated to be 1.28×10^{-3} [mm × s/m × kPa × day] (Mohammed, 2006), v_w = wind velocity at the water surface [m/d], e_s = saturated vapor pressure of a freshwater surface at air temperature [kPa], e_a = actual air vapor pressure [kPa] at dewpoint temperature, T_d = mean daily dewpoint temperature [°C], β = water activity coefficient that is a function of T_a = mean daily air temperature [°C], and C = salinity [g/L]. Additional details regarding the calculation of variables included in Eq. (12) are provided in the Supplemental Information S3.

Groundwater Contributions: Groundwater contributions are not adequately monitored at the GSL and little is known about the seasonal magnitude, distribution or salt concentration of Q_G . Based on limited data, [Zamora and Inkenbrandt \(2024\)](#) approximated a yearly total Q_G for the south arm ($Q_{G,S}$) = $0.17 \text{ km}^3/\text{yr}$ with concentration ($C_{G,S}$) = 3.61 kg/m^3 and for the north arm ($Q_{G,N}$) = $0.34 \text{ km}^3/\text{yr}$ with concentration ($C_{G,N}$) = 3.06 kg/m^3 . Due to lack of lake wide monitoring, $Q_{G,S}$ and $Q_{G,N}$ were divided evenly to estimate a constant, daily value. $Q_{G,S}$ was further divided into $Q_{G,UBL}$ and $Q_{G,DBL}$. Various distributions were evaluated, values of $Q_{G,UBL}$ = $0.8Q_{G,S}$ and $Q_{G,DBL}$ = $0.2Q_{G,S}$ with $C_{G,UBL}$ and $C_{G,DBL}$ assumed to equal $C_{G,S}$ best matched historical WSE time series for the UBL and DBL and were incorporated herein.

Turbulent Diffusion: Eqs. (7–8) also included the bulk turbulent diffusion coefficient (E') at each time step i that was estimated per [Chapra and Martin \(2004\)](#):

$$E' = \frac{A_i E_i}{H_i} \quad (13)$$

where A_i = surface area of the DBL/UBL interface [m^2], H_i = depth of the south arm [m], and E_i = turbulent diffusion coefficient across the UBL/DBL interface [m^2/d] ([Chapra and Martin, 2004](#)):

$$E_i = \frac{E_0}{(1 + aR_i)^{0.5}} \quad (14)$$

where E_0 = maximum diffusion coefficient [m^2/d], a = a tuning coefficient, and R_i = Richardson number. The maximum diffusion coefficient was calculated using ([Sundaram and Rehm, 1973](#)):

$$E_0 = cU^* \quad (15)$$

where c = a tuning coefficient and U^* = shear velocity [m/s]; c was calculated at each time step using ([Chapra and Martin, 2004](#)):

$$c = \frac{WSE_s - H_0}{b} \quad (16)$$

where WSE_s = daily WSE of the south arm [m], and H_0 = lowest point along the lakebed within the south arm [m], equal to 1270 m ([Root, 2023](#)), and b = a tuning coefficient. Both a and b became the primary tuning coefficients used to calibrate mass transfer between the south arm layers during model calibration. U^* was taken as ([Chapra and Martin, 2004](#)):

$$U^* = \sqrt{\frac{\rho_{air} C_d v_w^2}{\rho}} \quad (17)$$

where ρ_{air} = density of the air (assumed equal to 1.2 kg/m^3), C_d = dimensionless drag coefficient (assumed equal to 1.3×10^{-3}), v_w = wind speed at model time step i [m/s], and ρ = density of the water [kg/m^3]. The Richardson number, R_i , a dimensionless number that parameterizes competition between buoyancy and shear forces generated through the water column, was calculated using ([Ford and Johnson, 1986](#)):

$$R_i = -\frac{\left(\frac{g}{\rho}\right) \left(\frac{dp}{dz}\right)}{U^* / (z_s - z)^2} \quad (18)$$

where g = acceleration due to gravity (i.e., $9.81 \text{ [m/s}^2]$), dp/dz = gradient of density with depth, z_s = WSE of the south arm [m] and z = elevation at which the R_i is computed [m], in this case at the DBL/UBL interface. The ρ gradient at DBL/UBL interface was computed with a finite divided difference ([Chapra and Martin, 2004](#)):

$$\frac{d\rho}{dz} = \frac{\rho_i - \rho_{i+1}}{z_i - z_{i+1}} \quad (19)$$

where ρ_i = density of the UBL [kg/m^3], ρ_{i+1} = density of the DBL [kg/m^3], z_i = elevation of the midpoint of the UBL [m], and z_{i+1} = elevation at the DBL midpoint [m].

North/South Exchange Flows: To calculate Q_{NS} and Q_{SN} as a function of lake conditions and New Breach berm geometry, an analytical formulation was developed based upon a USGS New Breach velocity profile dataset (from an ADCP up-looker) that allowed for consideration of four flow scenarios: 1) a no-flow case (berm height exceeds water surface elevation), 2) the most common bidirectional flow scenario (Q_{NS} and Q_{SN}), 3) unidirectional flow Q_{NS} , and 4) unidirectional flow Q_{SN} . From January 2017 to June 2022, the berm was at its lowest elevation of 1275 m. In July 2022, it was raised to a medium elevation of 1276.2 m and in February 2023 it was raised to its highest elevation of 1277.7 m, fully segregating the arms.

The analytical formulation used energy conservation via Bernoulli's equation in a one-dimensional formulation of specific energy, referencing berm height, water surface elevations, ρ of the lake arms, and the location of the flow interface between the exchange flows, to estimate Q_{NS} and Q_{SN} via empirical rating curves fit to New Breach Q ([Dutta et al., 2024](#)):

$$Q_{NS} = 2.4H_I^{1.7}; \text{ for berm elevation} = 1275 \text{ m} \quad (20)$$

$$Q_{NS} = 1.08 \times 10^{-8}(H_I - 2.97)^{14.97}; \text{ for berm elevation} = 1276.2 \text{ m} \quad (21)$$

$$Q_{SN} = 4.51(H_T - H_I)^{1.64}; \text{ for berm elevation} = 1275 \text{ m} \quad (22)$$

$$Q_{SN} = 1.85(H_T - H_I)^{0.97}; \text{ for berm elevation} = 1276.2 \text{ m} \quad (23)$$

where Q is in [m^3/s], H_I = flow interface between NS and SN flow, and H_T = height of the water flowing over the berm [m]. The flow interface was calculated using:

$$H_I = \frac{\rho_N H_N - \rho_S H_S}{\rho_N - \rho_S} - \frac{C_{NS} V_{NS}^2 \rho_N}{2g(\rho_N - \rho_S)} + \frac{C_{SN} V_{SN}^2 \rho_S}{2g(\rho_N - \rho_S)} \quad (24)$$

where ρ_N = density of the north arm [g/cm^3], ρ_S = density of the south arm (assumed to be density of the UBL) [g/cm^3], H_N = height of the north arm water surface [m] above the bottom of the New Breach (elev. 1272.9 m), and H_S = height of the south arm water surface [m] above the bottom of the New Breach, V_{NS} = average NS flow velocity [m/s], V_{SN} = average SN flow velocity [m/s] (both V_{SN} and V_{NS} required iterative calculation), g = gravitational constant [m/s^2], and C_{NS} , C_{SN} = dimensionless coefficients to correct for friction loss and non-uniformity. For the 1275 m berm, $C_{NS} = 1.71$ and $C_{SN} = -1.84$. For the 1276.2 m berm, $C_{NS} = 19.34$ and $C_{SN} = -0.43$. These coefficients are dependent on berm elevation and were developed by comparing flow interface calculations to the USGS ADCP velocity data (Dutta et al., 2024). The height of the water above the berm was calculated using:

$$H_T = H_S - \frac{C_{SN} V_{SN}^2}{2g} \quad (25)$$

Since the calculations of H_T and H_I include an average flow velocity (V) that is a function of Q , an iterative procedure was implemented where H_S was used as an initial value for H_T and an initial value of H_I was calculated using:

$$H_{I,initial} = \frac{\rho_N H_N - \rho_S H_S}{\rho_N - \rho_S} \quad (26)$$

Eqs. (20–23) were then solved to obtain Q_{NS} and Q_{SN} .

For the 1277.7 m berm case, with sufficient WSE, flow scenario 4 (unidirectional flow north) may occur and the berm was treated as a broad-crested weir:

$$Q_{SN} = C_w L H_S^{1.5} \quad (27)$$

where C_w = weir discharge coefficient, equal to 1.6 and calibrated based on USGS discrete Q measurements at the New Breach, L = length of berm, equal to 30.5 m, and H_S is in [m]. These equations are a significant simplification of the hydraulics occurring at the New Breach but do cover the historic ranges of geometric conditions of the submerged berm.

An adjustment to these empirical rating curves was performed before incorporation into the model. Eqs. (20 – 23) and Eq. (27) were applied over their corresponding time periods (7/1/2017 – 7/21/2022 for low elev. 1275 m, 7/22/2022 – 2/13/2023 for medium elev. 1276.2 m, and 2/14/2023 – 9/30/2023 for high elev. 1277.7 m). Historical observations of ρ and WSE for the UBL and north arm from the calibration/validation datasets were used as inputs to the rating curves. The outputs were then compared against discrete measurements of Q_{NS} and Q_{SN} at the New Breach, which were compiled from NWIS (USGS, 2023) and linearly interpolated to prepare a daily series. The average daily difference between the predicted and observed Q_{NS} and Q_{SN} was calculated for each berm elevation and reported as a percentage of the predicted. The resulting percent error and daily correction was computed as:

$$Q_c = Q + Q \%_d \quad (28)$$

where Q_c = corrected Q [m^3/d] and $\%_d$ = percent difference, unique to each berm elevation and flow direction. The root mean squared percent error (RMSPE) for the raw and corrected rating curve outputs were compared and observed Q values were calculated over the entire time series to evaluate the performance of this adjustment, quantify prediction residuals, and validate its use within the USU-MBM. Additional details regarding rating curve performance are included in the Supplemental Information S5 (Fig. S5).

2.3. Data preparation

2.3.1. Forcing data preparation

Forcing data included Q and C of river inflows, P_d over the lake, yearly withdrawals from the mineral extraction activities, and the climatic variables used in estimating E_d (Dunn, 2025). During the simulation period, Q and C data for BR, WR, FB, GD, and Lakeside were compiled from the USGS National Water Information System (NWIS) database (USGS, 2023) using the data retrieval package in python (Horsburgh et al., 2022). 15-minute continuous Q observations were available for BR, WR, FB, and GD while discrete measurements of Q at Lakeside Breach were taken approximately every two months (Table S3, Fig. S2). The continuous Q data was averaged over each day while the discrete measurements at Lakeside were linearly interpolated to provide a daily time series for each

site.

Previous GSL models used Q_{BR} data from the USGS gage on the BR at Corinne, UT (10126000) approximately 42 km north and west of the BR-GSL confluence at BR Bay bridge. However, increases/decreases in Q and salt mass loading occurred between this gaging station and the BR Bay bridge (10010060) due to lateral stream inflows, influences of the BR Migratory Bird Refuge, and infiltration through the berms separating the evaporation ponds from either side of BR Bay. Therefore, a correction was performed in this study using a seasonal, piecewise linear regression between the day of the water year and the difference between discrete Q measurements made at the BR Bay bridge and daily BR gage Q (Supplemental Information S2, Fig. S3). RMSPE was calculated for the corrected and uncorrected BR gage Q compared to the BR Bay bridge discrete Q measurements to determine the effectiveness of this correction.

C of the flows from the BR, WR, GD, and FB was not directly measured; therefore, water quality data that included specific conductance (SC) and ρ was compiled from NWIS (USGS, 2023) and converted to C in g/L (Supplemental Information S1, Fig. S2, Table S1). 15-minute continuous SC data was available for water years 2019, 2022, and 2023. Any gaps in the SC data for these sites were filled with ρ observations taken from samples collected monthly. A daily average of the continuous C data was performed; additional gaps in C time series were linearly interpolated between measurements. While ρ at the BR Bay bridge was generally higher than at the BR gage, there was no clear trend to formulate an appropriate ρ correction. Instead, ρ at the BR Bay Bridge was prioritized; any gaps were filled with data provided from the BR gage.

Since 2017, four companies have harvested minerals including Cargill Salt Inc., Morton Salt Inc., and U.S. Magnesium LLC from the south arm and Compass Minerals from the north arm. Yearly withdrawals for each mineral company were compiled from a public USU dataset (Tarboton, 2024). Detailed information on the extraction operations is privately held, thus for this study, published yearly withdrawal V from each company corresponding to each side of the GSL was divided evenly across days within the year to calculate constant, daily $Q_{m,out}$. Daily P_d data was obtained from Oregon State University's PRISM Climate Group (Daly et al., 2008) using Climate Engine (Huntington et al., 2017). The data was reported at a 4 km grid resolution. Cells falling over the GSL were identified using a GSL lake shapefile provided by Tarboton (2024) and the data within each cell was averaged to produce a daily time series of P_d for use in Eq. (10).

Hourly climate data including v_w , T_d , site pressure (p_{site}), maximum daily air temperature ($T_{a,max}$), and minimum daily air temperature ($T_{a,min}$) was obtained from Utah State University's Utah Climate Center (USU, 2024) from three sites on the GSL (Fig. S2, Table S2). Wind data at 15-minute intervals (v_w) was also measured by the USGS at the New Breach and compiled from NWIS (USGS, 2023; Table S2). A daily average was applied to the continuous data at individual collection sites. After evaluating the spatial variance of the datasets across the collection sites, a single, spatial average value for each variable was generated and understood to be representative of GSL conditions (Supplemental Information: Fig. S4).

2.3.2. Calibration and validation data preparation

Historical observations of C , V , and calculated M for each control volume were gathered over the entire simulation period to establish initial conditions for the model and to calibrate and validate the USU-MBM (Dunn, 2025). Historical UBL, DBL and north arm C were derived from sample ρ , SC and T data while the UBL C dataset also included percent salinity (%C) measurements (Supplemental Information S1, Table S1). ρ and T data were compiled from NWIS (USGS, 2023), the Utah Geological Survey's (UGS) Brine Chemistry Database (Utah Geological Survey, 2020), and water quality monitoring reports from HDR Engineering published by the Utah Department of Water Quality (2022). Five sites were available for the north arm, eleven sites reported UBL and DBL samples and eighteen sites reported just UBL samples (Table S1, Fig. S2). DBL and UBL SC data was collected at two sites in the south arm by the Brine Shrimp Cooperative (BSC) and published in Brown et al. (2023) while the Department of Wildlife Resources (DWiR) collected %C measurements of the UBL at 15 sites. Additional details on the collection and analytical methods each entity used to develop these datasets are documented in Dunn et al. (2025).

To test the ability of the modeling approach to reproduce DBL and UBL C and V a depth to DBL dataset developed by the USGS (using SC profiles taken at one site in Carrington Bay and one site in Gilbert Bay) was used to curate C , V and an interface elevation time series for the UBL and DBL (McIlwain et al., 2023). Daily DBL/UBL interface elevations were calculated individually for Carrington Bay and Gilbert Bay by linearly interpolating between observations of DBL depths and subtracting from daily, historical south arm WSE observations.

To curate the C time series, C measurements above the calculated DBL interface within each bay were apportioned to the UBL; all data below the interface were assigned to the DBL. Weighted averaging of respective profiles was performed and C measurements were supplemented using linear interpolation to develop daily time series at each sampling location. Daily median UBL, DBL and north arm C were calculated by averaging across sites, based upon observed spatial homogeneity. Without additional data, these time series are considered representative of conditions within each control volume in the model.

Measurement uncertainty, the combination of multiple independent data sets, various C conversion equation applications, and the spatial homogeneity assumption introduced uncertainty into the calibration/validation datasets. It is necessary to keep these uncertainties in mind when evaluating USU-MBM performance; therefore, the total standard deviation (σ_T) in the datasets due to each source of uncertainty was calculated and then used to develop 90 % confidence intervals (CI) for the representative C time series for each control volume. These intervals were applied to the representative time series and used to evaluate USU-MBM performance during the model formulation and calibration processes.

Dunn et al. (2025) reported σ_T and a 90 % CI for the UBL dataset. DBL and north arm confidence intervals were calculated herein following the same method, where a first order error analysis was performed to calculate σ_T for the DBL and north arm C time series. The daily north arm dataset only included ρ observations, thus variance in the north arm dataset was primarily due to spatial averaging and measurement uncertainty. The average standard deviation (σ) across all north arm sites during the entire modeling period and the

C resulting from the reported ρ measurement accuracy was included in the σ_T calculation. The DBL dataset included ρ and SC data, thus it was broken into two subsets, one for each variable, to isolate spatial variation. Average σ over space and σ resulting from measurement uncertainty were calculated for each data type. Variance from combining datasets for the DBL was also explored by calculating average σ between the daily time series at BSC (Northwest)/USGS (2565) and BSC (South)/USGS (3510) measurement sites.

Continuous, 15-minute observations of north and south arm WSE were available from NWIS (USGS, 2023; Table S2). The continuous data was averaged to determine daily WSE for both arms. The USGS reported a ± 3 cm accuracy in their WSE data that was used to calculate a 90 % CI surrounding the historical WSE time series. This confidence interval was applied to the daily, historical WSE time series for the UBL and north arm when comparing USU-MBM outputs to the historical observations. The USU-MBM considered Gilbert and Carrington Bays as single UBL/DBL control volumes; however, DBL elevation differed slightly between the south arm bays. Thus, a representative DBL elevation was calculated to evaluate DBL model outputs. The USGS WSE/A/V tables (Root, 2023) were used to convert historical time series of DBL elevation to DBL V within each bay. The volumes were summed to get total DBL V within the south arm; this V was then related to south arm WSE to produce a representative DBL elevation.

The curated historical WSE time series were converted to V using the USGS WSE/A/V tables (Root, 2023). UBL V was calculated by subtracting total DBL V from total south arm V. Combining the C and V time series, daily M was then calculated for the UBL, DBL, and north arm using (Chapra, 1997):

$$M_i = V_i \times C_i \quad (29)$$

where M_i is in [kg], V_i is in [m^3], and C_i is in [kg/m^3] for any given layer. The published uncertainty in USGS WSE data (± 3 cm) was converted to V using the USGS tables. Combining uncertainties from the V and C time series, relative uncertainty in daily M was determined using (Berthouex and Brown, 2002):

$$\frac{\sigma_{M_i}}{M_i} = \sqrt{\left(\frac{\sigma_{C_i}}{C_i}\right)^2 + \left(\frac{\sigma_{V_i}}{V_i}\right)^2} \quad (30)$$

where σ_{M_i} = standard deviation of the M within a given layer, \bar{M}_i = average M within a given layer, $\left(\frac{\sigma_{C_i}}{C_i}\right)^2$ = total, relative variance in C for a given layer, and $\left(\frac{\sigma_{V_i}}{V_i}\right)^2$ = total, relative variance in V for a given layer. A daily confidence interval for M was then calculated for use in evaluating USU-MBM performance.

2.4. Model calibration and validation

Based on historical observations, the DBL experienced abrupt increases and decreases in volume immediately following the opening of the New Breach (January – July 2017). Therefore, the beginning of the calibration period began July 2017 under stable DBL conditions. December 2021 was selected as the end of the calibration period to provide a sufficiently long validation period to evaluate the USU-MBM's performance for all three constructed berm elevations. After model calibration and validation, root mean squared errors (RMSE) and Nash-Sutcliffe efficiencies (NSE) were calculated for each output to evaluate model performance. Model residuals were also analyzed to provide insight into potential biases, including shortcomings due to input data limitations and a short historic record.

Model calibration focused first on addressing underprediction in north arm WSE. E_d was selected as the WSE calibration parameter because Eq. (12) was documented to overestimate E_d under extreme C conditions (Mohammed and Tarboton, 2012). A percent reduction in E_d was only explored for the north arm (% E_N) due to its extremely high C. Values for % E_N ranging from 0.5 to 0.95 were tested by performing model runs and calculating RMSE over the calibration period. A 10 % reduction (% E_N = 0.9) was selected and applied during the summer months (May to August) which resulted in the lowest RMSE value between observed and predicted north arm WSE (Table 1).

The tuning coefficients a and b used in the turbulent diffusion coefficient calculations (Eqs. 14–15) were then calibrated to account for the hypersaline nature of the GSL, addressing error in south arm M partitioning that was affecting C predictions. The USU-MBM was run over the calibration period with a incremented within the suggested range of [10, 30] (Chapra and Martin, 2004). Chapra and

Table 1
Calibrated parameters and constants used in the USU-MBM.

Variable	Value	Units
a	10	-
b	6.8	-
% E_N	0.9	-
g	9.81	m/s^2
Cd	1.3×10^{-3}	-
ρ_a	1.2	kg/m^3
C_{sat}	275	g/L

Martin (2004) suggested $b = 34$; however, due to the extreme ρ of GSL waters, a range of b values was explored by incrementing b between 5 and 40 to determine a GSL-specific value. Based on RMSE results, the optimum a and b were 10 and 6.8, respectively (Table 1).

Terminal lakes typically exhibit long residence times; thus, model validation was performed as an extension of the calibration period to avoid initial condition biases that might mask model performance. RMSE and NSE values during the validation period were calculated for the north arm, UBL, and DBL elevations (derived from V_N , V_S , and V_{dbl}) and C_{dbl} , C_{ubl} , C_N . Due to this methodology, when evaluating RMSE and NSE results it is important to note that any propagated errors passing through the calibration period are maintained and captured within the validation period.

2.5. Impact of forcing data error

USU-MBM performance is affected by the accuracy of the forcing data and the methods used to calculate Q_{NS} , Q_{SN} , Q_{BR} , $Q_{G,ubl}$ and $Q_{G,dbl}$. An error analysis was performed to understand how these errors propagate through the system by running a series of model simulations. The entire simulation period was considered to ensure USU-MBM sensitivity was evaluated under all Q , climatic, and New Breach submerged berm conditions. Each mass balance term was either increased or decreased individually within a given simulation based on the upper and lower bounds of the associated error. Q_{NS} and Q_{SN} were also considered in unison, the upper range of error in Q_{NS} was paired with the lower range of error in Q_{SN} ($+Q_{NS}$, $-Q_{SN}$) and vice versa ($+Q_{SN}$, $-Q_{NS}$) to understand the impacts of uncertainty in net New Breach flows.

Precipitation had a reported $\pm 10\%$ error based on analysis performed by Daly et al. (2008). Error in surface water Q and C , excluding corrected Q_{BR} , was based on values documented by the USGS: $\pm 5\%$ for Q (Oberg et al., 2005), $\pm 0.001 \text{ g/cm}^3$ for ρ (USGS, 2006) and $\pm 5\%$ for SC (USGS, 2019). Climate data errors due to instrumentation accuracy reported within manufacturer documentation were determined to be $\pm 0.5^\circ \text{C}$ for T , $\pm 0.3 \text{ m/s}$ for v_w , and $\pm 0.3 \text{ hPa}$ for p_{site} (University of Utah, 2024). For the Q_{NS} , Q_{SN} , and Q_{BR} correction, the RMSPE of the corrected time series was designated while various distributions of south arm groundwater flow were evaluated including: $Q_{G,dbl} = Q_{G,S}$ with $Q_{G,ubl} = 0$, $Q_{G,dbl} = 0.5Q_{G,S}$ with $Q_{G,ubl} = 0.5Q_{G,S}$, and $Q_{G,dbl} = 0.9Q_{G,S}$ with $Q_{G,ubl} = 0.1Q_{G,S}$. The RMSE for C_{UBL} between each simulation and historical model results was calculated to 1) determine the most effective ways to improve the USU-MBM and 2) establish the sensitivity of various data sets on model performance to inform future monitoring efforts at the GSL.

2.6. Management scenarios

With the calibrated USU-MBM, simple management scenarios were formulated to exemplify the model's ability to simulate berm management strategies and to explore how adaptations to the New Breach berm might affect UBL C . For this effort, three simulations

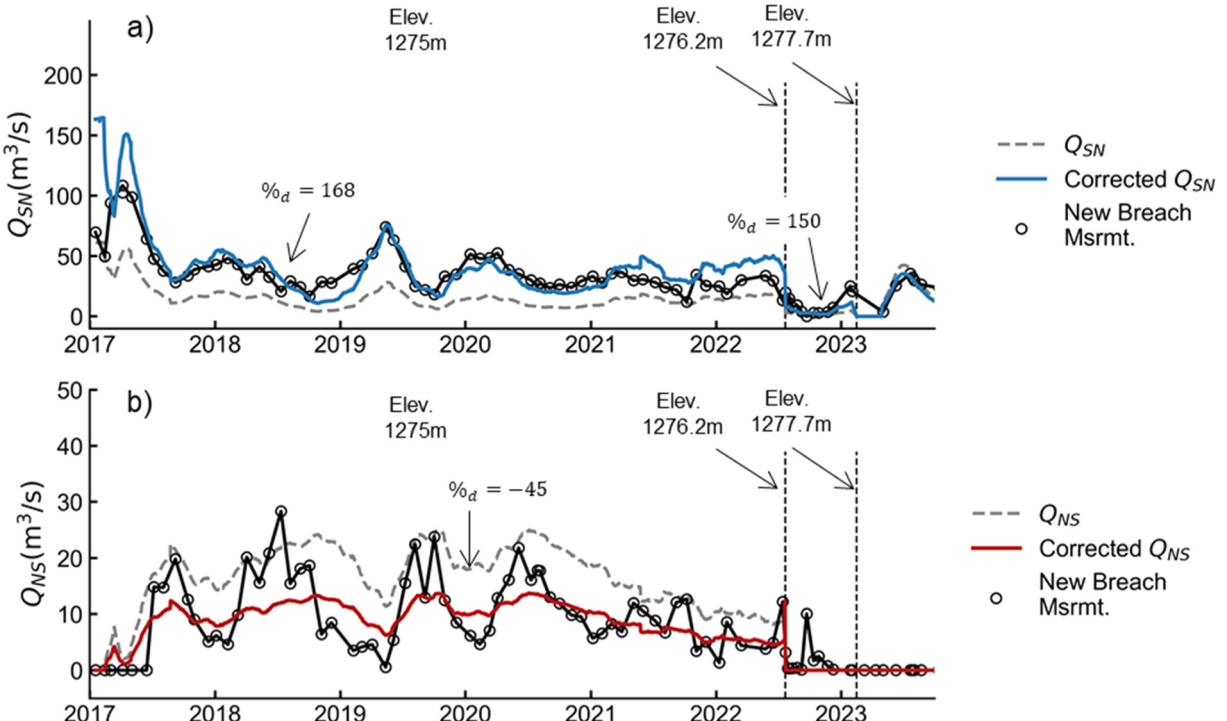


Fig. 3. New Breach rating curve correction results for (a) Q_{SN} and (b) Q_{NS} .

were performed: 1) the berm was at a low elevation of 1275 m throughout the entire simulation period, 2) the berm at a medium elevation of 1276.2 m, and 3) the berm at a high elevation where the south arm is fully isolated, 1279 m. These berm conditions were chosen to isolate the effect each berm elevation has on C and WSE over the range of conditions experienced at the lake since the New Breach was constructed. UBL C outputs from each of the three simulations were compared against the simulation of historical conditions that incorporated a low berm elevation July 2017 – June 2022, medium berm July 2022 – February 2023, and berm elevation 1277.7 m February 2023 – September 2023. This comparison was made to evaluate the influence of each berm paradigm, the efficacy of previous adaptive management decisions, and the success of the berm as a management tool.

3. Results

3.1. Rating curve adjustment

After analyzing the performance of the discharge rating curves during USU-MBM formulation, the 1275 m and 1276.2 m berm equations were found to underestimate Q_{SN} , while the 1277.7 m equation performed well (Fig. 3a), necessitating a positive correction factor for the 1275 m and 1276.2 m Q_{SN} predictions (1.68 and 1.5, respectively). For Q_{NS} , the 1275 m equation predictions were in good agreement with peak Q observations, but failed to predict the low Q_{NS} values, requiring a negative correction factor (-0.45). The 1276.2 m Q_{NS} equation slightly underestimated observed Q_{NS} (Fig. 3b); however, the disparity was small thus the 1276.2 m Q_{NS} equation was not corrected. Historically, when the berm is at 1277.7 m, Q_{NS} is zero, therefore, no correction factor was calculated for this case. The raw Q_{SN} rating curve outputs across all berm conditions had an RMSPE of 157 % while the corrected Q_{SN} RMSPE was 67 %. For Q_{NS} , the uncorrected RMSPE was 184 % and the corrected RMSPE was 85 %, showing that these corrections improved rating curve performance for both flow directions throughout the entire simulation period. Additional details regarding rating curve performance vs observed Q_{NS} and Q_{SN} are presented in the [Supplemental Information S5, Fig. S5](#). The complex exchange flow mechanisms and on-site conditions, including the berm geometry and composition, are not fully captured in the model and result in discharge residuals for the north arm that cannot be further corrected at this time. Additional research and more advanced hydraulic modeling is merited.

3.2. Data preparation

Time series of the forcing data (Fig. 4, Fig. S3) showed that the smallest contributor of inflow volume to the GSL was Q_{GD} , followed by Q_L , Q_{WR} , then Q_{FB} while the largest contributor was Q_{BR} (Fig. 4c). ∇ gained via P_d can exceed surface water inflow volumes during storm events but does not cumulatively contribute more ∇ than the GSL tributaries (Fig. 4a). More north arm brine was pumped out of

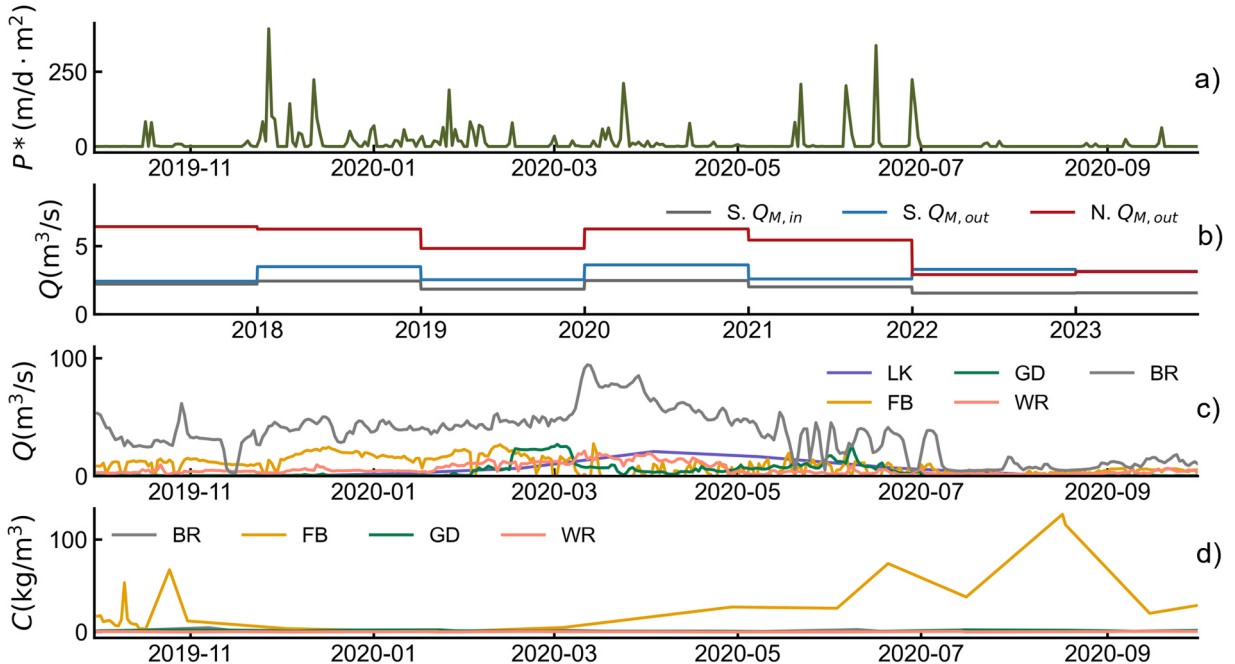


Fig. 4. Daily time series of the prepared forcing data from water year 2020 including (a) precipitation (P^*), (b) withdrawal and return flows from the mineral extraction activities, (c) River Q and (d) River C of the surface water Q. Mineral extraction withdrawal data from the north arm, $N. Q_{M,out}$, and south arm, $S. Q_{M,out}$, and return flow to the south arm, $C. Q_{M,in}$ (b) is shown for the entire simulation period to showcase yearly shifts in flow volumes from these activities. P^* has units of m^3/s derived by multiplying P_d by surface area of the lake at each time step.

the GSL ($N. Q_{M,out}$) than south arm brine ($S. Q_{M,out}$) while return flows ($S. Q_{M,in}$) were similar to inflow volumes from GD (Fig. 4b, c). Given the large contribution of flow from the BR compared to other river inflows, it was necessary to apply a correction to the BR gage data to better account for the significant deviation in Q_{BR} between the BR gage and the BR Bay Bridge (Fig. S3). Finally, of the surface water inflows, FB had the highest C before entering the south arm while all other inflows exhibited relatively low C (Fig. 4d).

A first order error analysis was performed on C_{UBL} , C_{DBL} , and C_N from the calibration/validation datasets to consider uncertainties associated with the prepared data. 90 % CI for the UBL was ± 12 g/L as discussed in Dunn et al. (2025), ± 42 g/L for the DBL, and ± 24 g/L for the north arm (Table 2). As expected, the largest source of uncertainty for the UBL came from combining varied types of salt concentration measures and limited spatial and temporal data (UBL $\sigma = 6.64$ g/L). For the DBL and north arm, the largest uncertainties resulted from averaging through space (DBL $\sigma = 18.8$ g/L, north arm $\sigma = 14.9$ g/L) (Table 2). Spatial variability within the DBL was the highest. This may be partially due to the depth to DBL dataset used to calculate DBL elevation within Carrington and Gilbert Bay which was derived using data from only one site in each bay. Because this dataset may not describe DBL elevation accurately at every point, an artificial decrease in the vertically averaged DBL C at sites where the DBL was shallower than recorded is probable. This exemplifies the need for increased monitoring of the DBL to deepen understanding of its dynamics and further evaluate modeling assumptions.

3.3. Model calibration and validation

3.3.1. Water surface elevation

A core objective in calibrating the USU-MBM was to evaluate and refine its ability to predict GSL WSE since the New Breach was opened (Fig. 5). WSE outputs during the calibration period for the north arm and UBL of the south arm generally showed good agreement with historical observations (south arm RMSE = 0.19 m and NSE = 0.73, north arm RMSE = 0.19 m and NSE = 0.67) suggesting that the calibrated model accurately accounted for most V fluxes in the system (Fig. 5a, b). However, analysis of the residuals revealed that the USU-MBM tended to overpredict UBL and north arm WSE (Fig. S6a, Fig. 6c). The calibration period RMSE for the DBL elevation was 0.23 m (Fig. 5c). In general, modeled and observed DBL elevation (and corresponding V) followed the same trend; however, the USU-MBM did not capture the abrupt shifts in observed DBL elevation during the calibration period. This is likely due to significant uncertainty in the historical DBL WSE time series because the depth to DBL dataset used to calculate historical DBL elevation had limited spatial and temporal resolution. Given these uncertainties, the accuracy of the predicted trend in DBL elevation during the calibration period suggests that the V threshold method is valid for use in partitioning V between the UBL and DBL and no further calibration was necessary.

Another core objective of the model was to capture WSE across varied New Breach berm conditions. During the validation period, the USU-MBM captured the seasonal trends in UBL and north arm WSE (UBL RMSE = 0.24 m and NSE = 0.91, north arm RMSE = 0.44 m and NSE = 0.87), but slightly underestimated both WSEs (Fig. 5a, b; Fig. S6b, Fig. S6d). The model overestimated DBL elevation during 2022 and predicted completed dissipation in September 2022, earlier than the dissipation observed in Carrington Bay in August 2023, but aligned with the dissipation observed in Gilbert Bay (Fig. 5c). This may be partially explained by severely restricting exchange flows at the New Breach via the berm raises and overestimation of mass transfer between the layers due to overestimation of shear velocity through the water column resulting from the underestimation of south arm WSE. These results showcase the calibrated model's ability to quantify New Breach exchange flows under a variety of berm geometries. They also indicate that the model relies on precise WSE predictions to accurately quantify NS flow through the New Breach and turbulent diffusion between the south arm layers, as demonstrated by the overestimates of DBL elevation. While WSE RMSE values during the validation period were higher than during the calibration period, they were influenced by errors propagated from the calibration period. These errors can be attributed to uncertainties in both the historical forcing data and limited temporal and spatial salinity data for the north arm and DBL.

Table 2

Average standard deviation (σ), total standard deviation (σ_T) and associated 90 % confidence interval for UBL, DBL, and north arm C .

Layer	Entity	Dataset	σ	${}^a\sigma_T$	90 % CI
^b UBL	BSC	YSI 556 Conductivity Meter			
	USGS, UGS, HDR	Anton Paar DMA 35 Density Meter	1.02		
	DWIR	Atago Master S28α Refractometer			
	BSC	SC		7.81	± 12.88
	USGS, UGS, HDR	ρ	3.97		
	DWIR	%C			
DBL	BSC, USGS, UGS	GSL site 3510, 2565	6.64		
	BSC	YSI 556 Conductivity Meter	1.44		
	USGS, UGS, HDR	Anton Paar DMA 35 Density Meter			
	BSC	SC		25.66	± 42.34
	USGS, UGS, HDR	ρ	18.80		
	BSC, USGS, UGS	GSL site 3510, 2565	17.41		
North Arm	USGS, UGS, HDR	Anton Paar DMA 35 Density Meter	1.36		
		ρ	14.89	14.95	± 24.67

^a σ is the average standard deviation from each type of error in the representative datasets while σ_T is the propagated error within each dataset

^b UBL σ and σ_T were taken from Dunn et al. (2025)

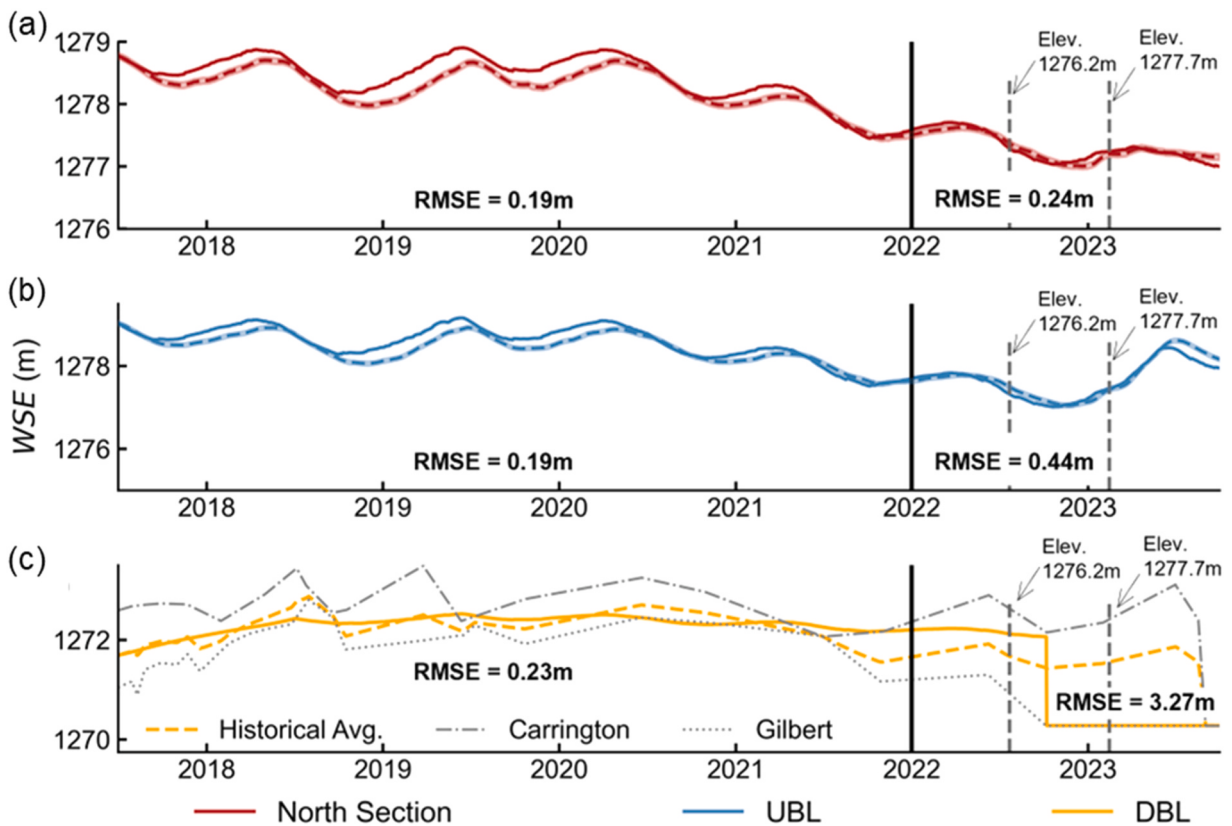


Fig. 5. WSE results for the north arm, UBL and DBL from the calibration and validation simulations. USU-MBM predictions are indicated by the solid lines while calibration/validation data is indicated by the dashed lines. North arm and UBL historical data are surrounded by the calculated 90 % confidence intervals indicated by the thin shaded regions. The DBL historical average was calculated as a volume weighted average between the Carrington Bay DBL elevation (gray dash-dot line) and the Gilbert Bay DBL elevation (gray dotted line). The black vertical line separates the calibration period (left) from the validation period (right) while the dashed gray lines indicate timing of New Breach berm raises.

3.3.2. Salt concentration

Accurate prediction of GSL C was another key objective for the USU-MBM, with a priority placed on the south arm due to current management priorities, as discussed previously. C outputs from the calibration period (Fig. 6) showed that UBL and DBL C matched the trend in the calibration data and fell well within the 90 % CIs (UBL RMSE = 6.8 g/L and NSE = 0.78, DBL RMSE = 10.6 g/L and NSE = 0.57). However, analysis of the residuals revealed that the USU-MBM underestimated C_{ubl} , underestimated C_{dbl} at lower concentrations, and overestimated C_{dbl} at higher concentrations (Fig. S7a, Fig. S7c). During the calibration period, predicted C_N followed a seasonal trend aligning with oscillations in V_N while historical C_N remained constant, sitting near the saturation threshold of water with respect to salt (north arm RMSE = 24 g/L and NSE = -15.25). This disparity suggests the USU-MBM did not fully capture the seasonal dynamics of M_N , indicated by interannual fluctuations in M_N , and explains the negative NSE value during this period (Fig. 7a). This would be expected given the limited temporal and spatial data for the north arm. Further, analysis of the residuals revealed that the model underpredicted C_N (Fig. S7e, Fig. S7f), thus there are likely unaccounted mass fluxes within the north arm. However, given the simplifications of the system, the closeness of fit suggests that the dominant M and V fluxes are represented in the USU-MBM and that it can positively replicate C observations within the UBL and DBL across a variety of hydroclimatic conditions.

During validation, the USU-MBM underestimated M_{ubl} , but overestimated C_{ubl} (UBL RMSE = 7.1 g/L and NSE = 0.82) due to underestimation of WSEs (Fig. 5b, Fig. 6b, Fig. 7b, Fig. S7b). These results indicate that for the USU-MBM, the trend in UBL C is dominated by WSE fluctuations. Conversely, C_{dbl} was overestimated during the validation period (DBL RMSE = 16.6 g/L) despite overestimation of WSE due to inaccurate estimates of M_{dbl} (Fig. 5c, Fig. 6c, Fig. 7c, Fig. S6d). The NSE values for C_{dbl} and C_N (DBL NSE = -0.84, north arm RMSE = 23.6 g/L and NSE = -18.7) during this period indicated that the model does not fully predict variance in the historical observations; however, the historical data is limited and the predicted C_{dbl} and C_{ubl} values fall within the 90 % confidence intervals associated with the time series. This exemplifies the model's ability to accurately predict south arm C under varied New Breach berm geometries and hydroclimatic conditions and further validates the methods used to partition M and V between the UBL and DBL.

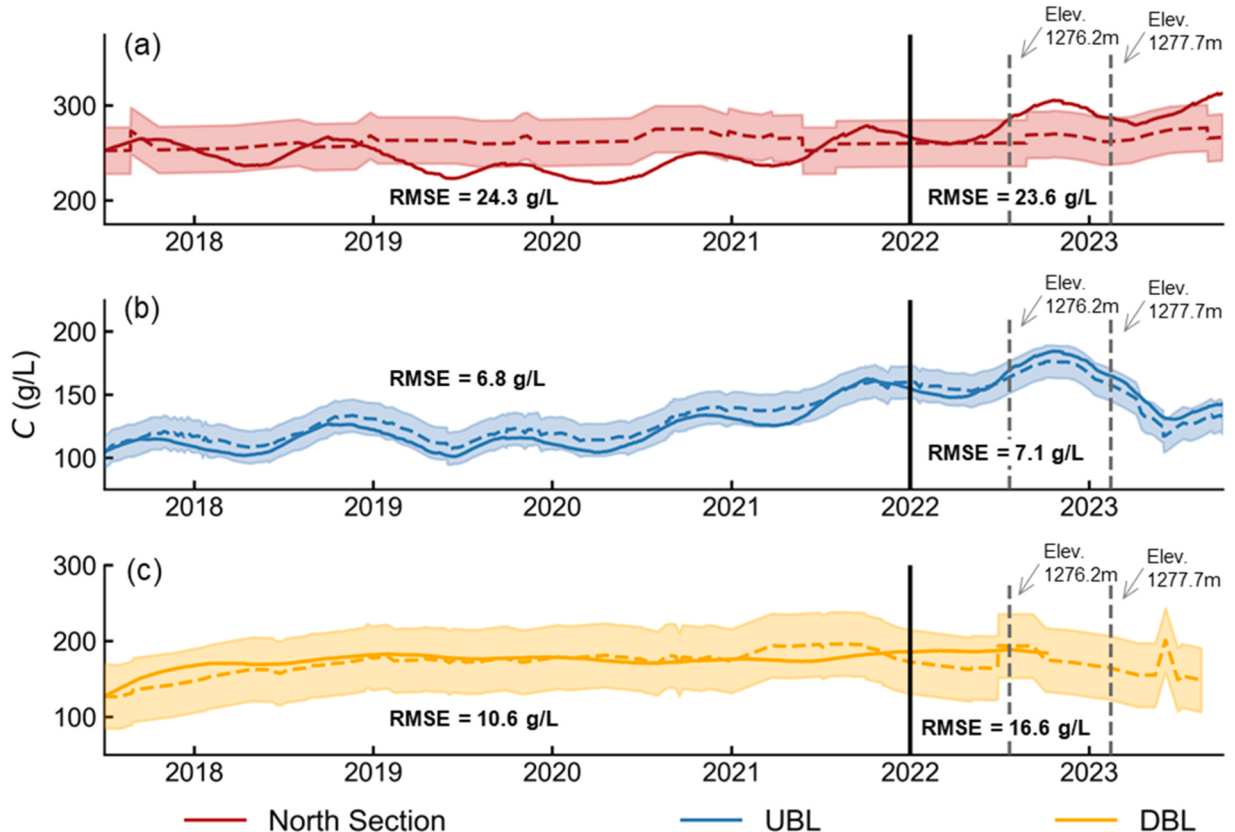


Fig. 6. Salinity (C) results for the north arm, UBL and DBL from the calibration and validation simulations. USU-MBM predictions are indicated by the solid lines while calibration/validation data is indicated by the dashed lines surrounded by calculated 90 % confidence intervals (shaded regions). The black vertical line separates the calibration period (left) from the validation period (right) while the dashed gray lines indicate timing of New Breach berm raises.

3.4. Impacts of forcing data error

The calibrated USU-MBM demonstrated a strong performance in predicting historical WSE and C despite uncertainties in 1) the forcing, calibration, and validation data, 2) assumptions used in quantifying mass balance terms, and 3) reliability of the available E_d , Q_G , and new breach flow methods. Regardless, the error analysis of forcing data provides insight concerning additional data collection priorities. Based on RMSE results, the USU-MBM was most sensitive to uncertainties in Q_{NS} , Q_{SN} , $Q_{BR,pred}$, $Q_{G,ubl}$ and $Q_{G,dbl}$ (Table 3; Fig. 8). It was hypothesized that the $+Q_{NS}$, $-Q_{SN}$ scenario would increase C_{UBL} since salt mass inflow via Q_{NS} was maximized and salt mass outflow via Q_{SN} was minimized and vice versa for the $-Q_{NS}$, $+Q_{SN}$ scenario. However, $+Q_{NS}$, $-Q_{SN}$ had a limited, but small decrease in C_{UBL} and $-Q_{NS}$, $+Q_{SN}$ resulted in a larger decrease in C (Fig. 8a). Mass loading to the UBL primarily resulted from mass transfer across the UBL/DBL interface due to the C gradient while UBL mass export occurred via Q_{SN} . When Q_{SN} is minimized, more M is retained causing C_{UBL} to be higher and mass transfer across the layers to be lower due to a decreased gradient. The decrease in M transfer across the layers into the UBL can offset the mass retention from decreasing Q_{SN} (Fig. 8a). This may also explain the observed trend in the isolated Q_{SN} simulation (Fig. 8d) where increasing Q_{SN} caused a slight increase in C_{UBL} while decreasing Q_{SN} decreased C_{UBL} . When Q_{NS} was isolated (Fig. 8c), maximizing Q_{NS} resulted in higher C_{UBL} and minimizing Q_{NS} caused lower C_{UBL} because increased M in the DBL heightened the C gradient between the layers escalating mass transfer from the DBL to the UBL.

Uncertainty in the New Breach Q rating curves is significant; however, C_{UBL} was most sensitive to the BR gage data regression (Fig. 8b; Table 3). Maximizing Q_{BR} caused lower C_{UBL} while minimizing caused higher C_{UBL} . It is also important to note that when Q_{BR} was minimized, the south arm WSE equalized with the north arm. The 1276.2 m Q_{SN} rating curve was developed only for unidirectional SN flow ($Q_{NS} = 0$), which only occurs when south arm WSE is higher than north arm WSE, thus these conditions were not captured in the simulation resulting in no predictions for C after July 21st, 2022. The USU-MBM was also sensitive to the distribution of south arm groundwater inflow into $Q_{G,ubl}$ and $Q_{G,dbl}$. When all south arm groundwater inflow was allocated to the DBL, it caused significant underprediction in C_{ubl} (Fig. 8e) and instability in C_{dbl} as indicated by the abrupt appearance and disappearance of the DBL (Fig. 8f). C_{ubl} was not significantly affected by the 90 % to UBL, 10 % to DBL or the 50:50 splits, however C_{dbl} was underpredicted under the 90:10 scenario.

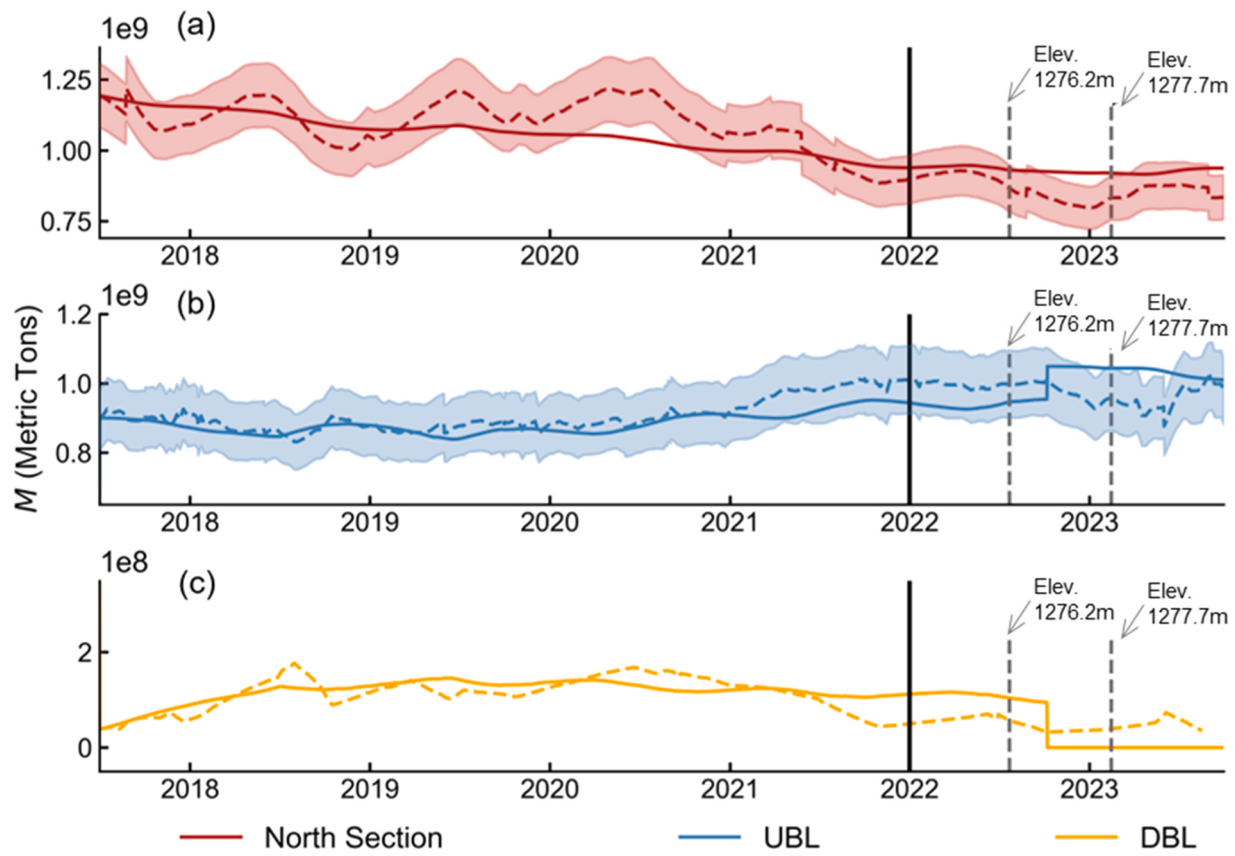


Fig. 7. Total Dissolved Salt Mass (M) results for the north arm, UBL and DBL from the calibration and validation periods. USU-MBM predictions are indicated by the solid lines while calibration/validation data are indicated by the dashed lines. North arm and UBL historical data are surrounded by the calculated 90 % confidence intervals (shaded regions). The black vertical line separates the calibration period (left) from the validation period (right) while the dashed gray lines indicate timing of New Breach berm raises.

Table 3

Ranges of error in GSL mass balance terms from the error analysis and the resulting RMSE values for UBL C when compared to historical conditions from July 2017 to October 2023.

Variable	Uncertainty	UBL C RMSE (g/L)	
		High	Low
Q_{BR}	±68 %	27.2	48.2
$Q_{WR,FB,GD,L}$	±5 %	1.1	1.1
$C_{WR,FB,GD}$	±0.001 g/cm ³	0.8	1.2
P_S, P_N	±10 %	2.9	3.0
E_S, E_N	±0.5 °C, ±0.3 m/s, ±0.3 hPa	4.3	4.4
Q_{NS}	±85 %	8.0	14.9
Q_{SN}	±67 %	2.4	6.8
+ Q_{NS} , - Q_{SN}	+ 85 %, -67 %	2.0	
- Q_{NS} , + Q_{SN}	-85 %, + 67 %	14.5	
	50 %, 50 %	0.7	
$Q_{G,ubl}, Q_{G,dbl}$	90 %, 10 %	0.1	
	0 %, 100 %	22.9	

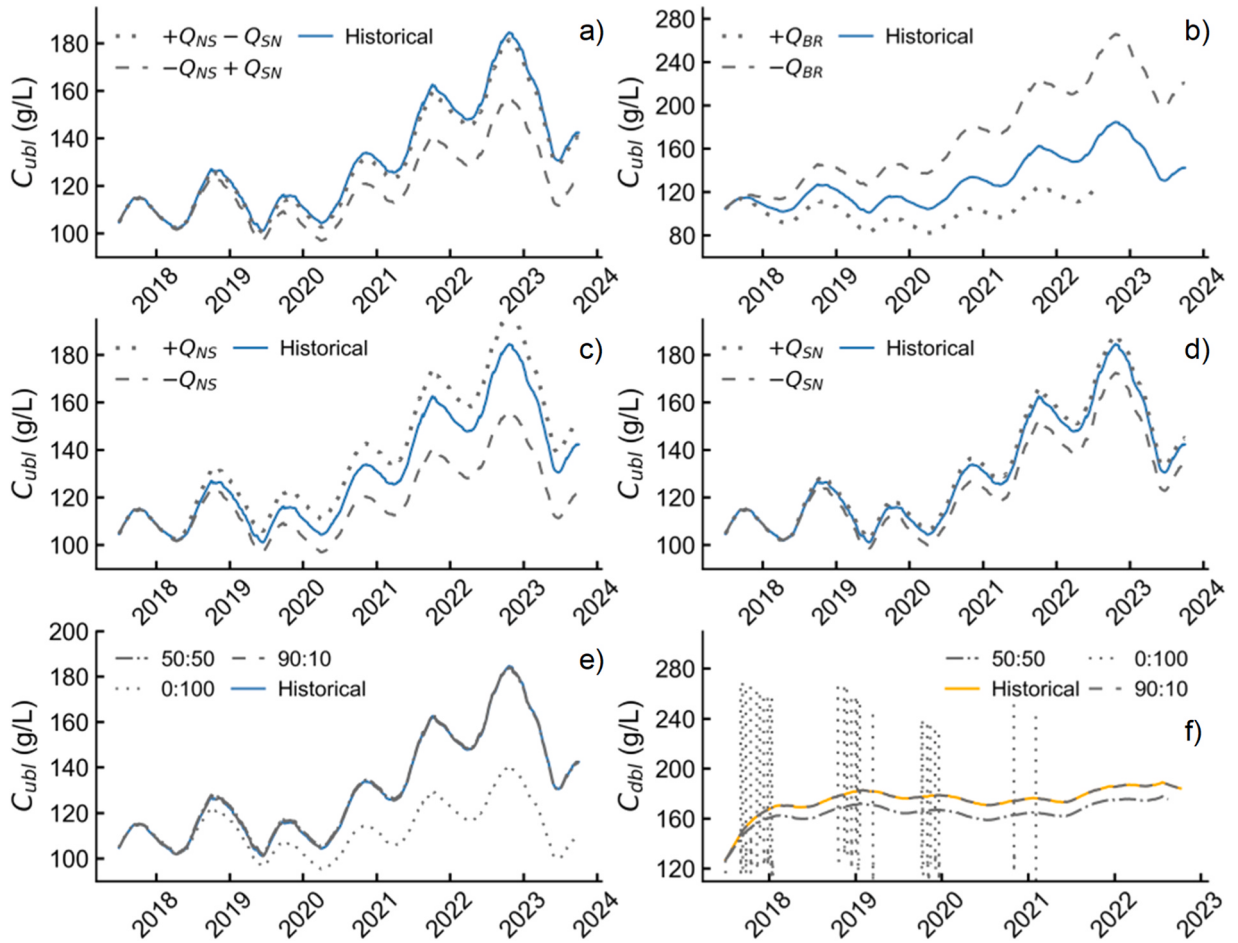


Fig. 8. C_{UBL} outputs from the forcing data error analysis applied to Q_{NS} and Q_{SN} in unison (a), Q_{BR} (b), isolated Q_{NS} (c), isolated Q_{SN} (d), and distribution of south arm groundwater inflow (e), and C_{DBL} output from south arm groundwater distribution analysis (f). In (e) and (f), 50:50 is the scenario where south arm groundwater inflow was distributed 50 % to the UBL and the DBL, 0:100 is the scenario where groundwater inflow was distributed 100 % to the DBL, and 90:10 refers to 90 % groundwater inflow to UBL and 10 % to the DBL. Horizontal, gray dotted lines in (f) indicate abrupt appearance and disappearance of the DBL in the 0:100 scenario.

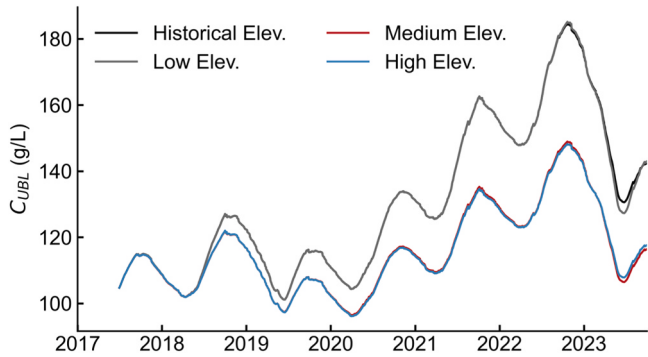


Fig. 9. UBL C outputs from the historical and management scenario simulations. Low Elev. refers to the berm at 1275 m for the whole period, Medium Elev. refers to the 1276.2 m berm elevation, High Elev. refers to the 1279 m berm elevation, and Historical Elev. refers to all three elevations as they occurred in the historical time period.

3.5. Management scenarios

Adaptive management at the GSL since the box culverts' closure and opening of the New Breach has focused primarily on altering the New Breach berm to control UBL C. An initial simulation was performed utilizing all three historical berm elevations with raises in berm elevation aligning with historical modifications, demonstrating the USU-MBM's ability to replicate historical New Breach flow conditions (Fig. 9). Three additional scenarios were run where each historical berm elevation was considered individually throughout the simulation period with no modification (Fig. 9). C outputs from all four berm conditions (historical, low berm elev. 1275 m, medium berm elev. 1276.2 m, high berm elev. 1279 m) did not deviate from each other until 2019 when the WSE began to decrease due to drought conditions and increased surface water diversions (Fig. 5). This indicates that C is more sensitive to New Breach exchange flows when river Q is lower. After 2020, C did not increase as drastically for the medium berm case compared to the historical and low berm cases due to maximized south arm mass export and minimal mass loading from the north arm. Despite mass loading restrictions from the north arm, the high berm case behaved similarly to the medium berm case. Consistent with the previous error analysis, these results indicate that blocking Q_{NS} may be the most effective use of berm adaptations and that the gain in V from isolating the south arm is offset by the retention in M for the upper brine layer. Further, UBL C, from the medium berm case simulation, was lower compared to the high berm case simulation beginning in spring 2023. This illustrates that keeping the berm at the medium elevation is a productive mechanism for maximizing salt export and minimizing salt import to the south arm.

4. Discussion

The USU-MBM builds upon past GSL models and studies by incorporating all available hydrologic datasets, new groundwater flux estimates, and recent prediction methods for New Breach exchange flows, to understand the role of various inflows, outflows, and historic management strategies on GSL level and salinity. This process-based approach accounts for the stratified south arm responses while improving water surface elevation and mass exchange estimates. Results from this study demonstrate the predictive strength of the USU-MBM, despite data limitations, while the error analysis highlighted potential future efforts for additional monitoring. The results also exemplify how this model can be applied to evaluate future scenarios and corresponding adaptive management decisions as it captured the complexities associated with the UBL/DBL and New Breach mass exchanges.

4.1. Model performance

4.1.1. Water surface elevation

Hydrologic observations at the GSL, particularly during the recent drought/flood cycle, have highlighted the connection between C and WSE. Thus, it is important to have accurate predictions of WSE to make informed, proactive management decisions for the lake to avoid additional negative impacts on GSL ecologic communities and economic production. The USU-MBM performed well in predicting WSE of the north arm and UBL, indicating that the model accounted for most water V fluxes in the system. However, consistent underestimates of WSE starting in 2021 are likely due to uncertainty in the forcing data. This may also be due to unknown inflows, uncertainty in groundwater contributions to the lake, and limited information regarding the quantity of return flows from mineral extraction activities during this period (Lukens et al., 2024). The error in WSE predictions could also result from uncertainty in the evaporation method or BR gage data correction. For the DBL, the RMSE values during calibration and validation were significant because the historical observations of DBL depth used to prepare the calibration data were limited spatially and temporally (measured three times per year on average). Development of the wind mixing algorithm was also severely limited by the temporal availability of the data which hindered the USU-MBM's ability to fully describe the complex hydrodynamics of south arm mixing. Due to these sources of uncertainty, increased hydrologic monitoring of surface water and groundwater inflows and DBL characteristics as well as improvement in E_d estimation methods are considered to be of high priority for future modeling and management efforts.

4.1.2. Salt concentration

Brine flies and brine shrimp are dependent on south arm C remaining within a healthy range ($100 < C_{ubl} < 160 \text{ g/L}$). If C_{ubl} falls outside this range, it affects individuals and population growth, which in turn affects the water and shore birds who feed on them (Mardene et al., 2020). This emphasizes the necessity of accurate predictions of UBL and DBL C. Modeled UBL C was within an appropriate range of uncertainty, but, as noted, C was primarily underestimated. The largest salt influx to the UBL is NS flow through the New Breach, thus the observed error in UBL C results mainly from error in estimates of north arm M and Q_{NS} . The most significant M flux into the DBL is Q_{NS} , thus poor predictions in DBL M and C are compounded by uncertainty in the New Breach Q rating curves. Since M transfer between the layers is dependent on the C gradient, low DBL C values and uncertainty in M export from the UBL via Q_{SN} further contributes to the low M and C predictions within the south arm. Causeway seepage also contributes M to the DBL (Jewell, 2021) but has not been thoroughly investigated and was not accounted for in the USU-MBM. Currents along the south arm lakebed have been observed (Naftz et al., 2014) that can lead to redissolution of precipitated salt and may be another relevant M flux that is not well understood, further explaining the model limitations.

4.2. Management scenarios

From the management scenario simulations, as expected, the berm was found to have the most influence on UBL C by altering mass flux. New Breach exchange Q was smaller than river Q values, showing that the berm has less effect on total lake V. However, when

focusing on salt concentration, the breach provides the largest mass flux in the system. This indicates that if south arm V gets too low and C gets too high, the berm should be used to minimize M import to the south arm via Q_{NS} and maximize M export via Q_{SN} by maintaining a medium elevation rather than fully isolating the south arm. This approach was taken by Utah Department of Natural resources who raised the berm by 1.2 m in July 2022. This action essentially shutoff all NS flow into the south arm which mitigated the effects of rapidly declining lake levels prior to the record low elevation recorded in November 2022. In contrast, the berm may not be as effective as perhaps assumed in increasing south arm C . If the berm is lowered, Q_{NS} will certainly increase, but Q_{SN} will also increase thus the net M in the south arm may not shift rapidly. The berm can and has been used as an emergency measure, such as the raise in February 2023, but long-term management of south arm C requires increases in river inflows to maintain the hydrologic balance of the GSL. Furthermore, sequestering salt in the north arm is an appropriate adaptive management strategy, but if too much is exported from the south arm, a series of wet years may cause the south arm to be too dilute ($C < 90 \text{ g/L}$), impacting the ecologic productivity of the brine shrimp communities (Utah Division of Forestry, Fire and State Lands, 2013).

4.3. Model utility and future work

The USU-MBM formulation successfully predicted GSL C and WSE, estimated New Breach exchange flows under varied berm elevations, and reproduced observed south arm salt stratification. However, as with any modeling tool, it is important to keep model assumptions and performance in mind when using it to inform lake management decisions. The USU-MBM is particularly useful in predicting long term C and WSE of the UBL and WSE of the north arm. The model requires limited input data which is beneficial for forecasting lake conditions. While further development and refinement of the New Breach rating curves would be beneficial, they are an important first step toward accurately estimating daily exchanges between the south and north arms within a lake wide model. Continuous monitoring of flow through the BR Bay Bridge may also improve estimates given the model's sensitivity to uncertainty in Q_{BR} and the impact of these inflows on south arm WSE and C . Additionally, increased monitoring of groundwater contribution, groundwater distribution between the UBL and DBL, and evaluation of evaporation estimates off hypersaline water bodies would also be valuable improvements. The USU-MBM did not incorporate a process-based method to partition V between the UBL and DBL due to limited data. It also did not consider the complex dynamics of salt precipitating from solution to the lakebed or reincorporation of salt mass due to seasonal fluctuations and changing WSE and shoreline. Thus, model formulation and performance could be improved by new hypersaline-specific developments based on data at appropriate temporal scales. Temperature effects on north arm M and contribution of salt mass to the south arm via causeway seepage should also be evaluated in the future to expand usage and accuracy of the USU-MBM.

Adaptive management strategies can also be developed using the USU-MBM, given its ability to estimate New Breach exchange flows. Similar to the model scenarios considered within this study, the USU-MBM can be used to explore the influence of varying the berm elevation and optimal timing for berm alterations. It could also be applied to a scenario-based framework that may consider climate and land use changes in addition to reallocation of water within the GSL basin. Since the USU-MBM had some limitations regarding north arm M dynamics, additional spatial and temporal monitoring along with more detail on withdrawals by the mineral industry would further improve USU-MBM estimates of north arm C . With the current USU-MBM formulation, future lake conditions could be evaluated by replacing the input data with climate and streamflow predictive models.

5. Conclusion

The primary purpose of this study was to develop an open access, process-based mass balance model of the Great Salt Lake to aid adaptive management efforts. Historical observations of C informed a model framework that includes control volumes for the two segregated lake arms, with the south arm further segregated into upper and lower brine layers. Key inflow V and M fluxes, bidirectional flow exchange occurring at the breach, and V and M partitioning between the south arm layers are tracked within the USU-MBM. With this simple formulation, the USU-MBM captured C and WSE in response to historic inputs of streamflow, climate, and adaptive management actions.

Based on results from this study, it was concluded that a two-layer model for the south arm is necessary to accurately predict UBL C , the magnitude of which has implications for the health of the ecologic communities. USU-MBM performance highlights several limitations of this study related to hydrologic monitoring for the entire lake and needed insights to quantify the physical processes in both arms as it relates to salinity. Additional spatial and temporal monitoring of water entering and evaporating from the GSL would further improve model estimates. This includes continuous monitoring of BR Bay Bridge inflows, increased monitoring of groundwater contributions, and detailed monitoring of withdrawals/effluents from the mineral industries. Temperature effects on north arm M , contribution of M to the south arm via causeway seepage, and evaporation of hypersaline water bodies should also be evaluated in the future to expand usage and accuracy of the USU-MBM.

A key feature of the USU-MBM is its ability to predict New Breach exchange flows given various berm elevations, the primary focus of adaptive management actions at the GSL. Based on USU-MBM application, it was concluded that using the berm to minimize mass import to the south arm and maximizing mass export to the north arm is the most productive mechanism for decreasing C within the UBL. Further, coupling the USU-MBM with predictive climate and streamflow models will enable forecasting GSL conditions under varying climate regimes. Since it has been shown that the USU-MBM can quantitatively evaluate adaptive management strategies, application of this tool will facilitate informed lake management decisions that aim to balance human, ecologic, and economic needs as conditions within and around the lake continue to change.

CRediT authorship contribution statement

Som Dutta: Writing – review & editing, Funding acquisition. **Bethany Neilson:** Writing – review & editing, Writing – original draft, Validation, Supervision, Resources, Methodology, Investigation, Formal analysis, Conceptualization. **Diana Dunn:** Writing – original draft, Visualization, Validation, Methodology, Investigation, Formal analysis, Data curation, Conceptualization. **Brian Crookston:** Writing – review & editing, Writing – original draft, Visualization, Validation, Supervision, Software, Resources, Project administration, Methodology, Investigation, Funding acquisition, Formal analysis, Data curation, Conceptualization.

Declaration of Competing Interest

The authors declare that they have no known competing financial interests or personal relationships that could have appeared to influence the work reported in this paper.

Acknowledgments

This study was funded by the State of Utah through the Department of Natural Resources—Forestry, Fire and State Lands (Grant # 204418) and through the Utah Water Research Laboratory at Utah State University.

Appendix A. Supporting information

Supplementary data associated with this article can be found in the online version at [doi:10.1016/j.ejrh.2025.102768](https://doi.org/10.1016/j.ejrh.2025.102768).

Data Availability

All model code and data are provided in an open access repository that is available at: <http://www.hydroshare.org/resource/267e083484a74866927d91bdef60f8d6>.

References

- AghaKouchak, A., Norouzi, H., Madani, K., Mirchi, A., Azarderakhsh, M., Nazemi, A., Nasrollahi, N., Farahmand, A., Mehran, A., Hasanzadeh, E., 2015. Aral Sea syndrome desiccates lake urmia: call for action. *J. Gt. Lakes Res.* 41 (1), 307–311. <https://doi.org/10.1016/j.jglr.2014.12.007>.
- Banks, J.R., Heinold, B., Schepanski, K., 2022. Impacts of the desiccation of the Aral Sea on the central asian dust life-cycle. *J. Geophys. Res. Atmospheres* 127, e2022JD036618. <https://doi.org/10.1029/2022JD036618>.
- Barnes, B.D., Wurtksbaugh, W.A., 2015. The effects of salinity on plankton and benthic communities in the Great Salt Lake, utah, USA: a microcosm experiment. *Can. J. Fish. Aquat. Sci.* 72 (6), 807–817. <https://doi.org/10.1139/cjfas-2014-0396>.
- Baxter, B.K., Butler, J.K., 2020. Climate change and Great Salt Lake. In: Baxter, B.K., Butler, J.K. (Eds.), *Great Salt Lake Biology*. Springer International Publishing, pp. 23–52. https://doi.org/10.1007/978-3-030-40352-2_2.
- Belovsky, G.E., Stephens, D., Perschon, C., Birdsey, P., Paul, D., Naftz, D., Baskin, R., Larson, C., Mellison, C., Luft, J., Mosley, R., Mahon, H., Van Leeuwen, J., Allen, D.V., 2011. The Great Salt Lake ecosystem (Utah, USA): long term data and a structural equation approach. *Ecosphere* 2 (3), art33. <https://doi.org/10.1890/ES10-00091.1>.
- Berthouex, P.M., Brown, L.C., 2002. *Statistics for Environmental Engineers*, 2nd Edition. LEWIS Publishers, Boca Raton, Florida.
- Bioeconomics, Inc., 2012. Economic significance of the Great Salt Lake to the state of utah. Prepared for the State of Utah Great Salt Lake Advisory Council, Salt Lake City, Utah. Retrieved from. <https://documents.deq.utah.gov/water-quality/standards-technical-services/great-salt-lake-advisory-council/activities/DWQ-2012-006864.pdf>.
- Borlina, C.S., Rennó, N.O., 2017. The impact of a severe drought on dust lifting in California's owens lake area. *Sci. Rep.* 7 (1), 1784. <https://doi.org/10.1038/s41598-017-01829-7>.
- Brown, P.D., Bosteels, T., Marden, B.T., 2023. Salt load transfer and changing salinities across a new causeway breach in Great Salt Lake: implications for adaptive management. *Lakes Reserv. Sci. Policy Manag. Sustain. Use* 28 (1). <https://doi.org/10.1111/lre.12421>.
- Chapra, S.C., 1997. *Surface water quality modeling*. McGraw-Hill Publisher, New York.
- Chapra, S.C., Martin, J.L., 2004. *Lake2k: A Modeling Framework for Simulating Lake Water Quality (Version 1.2)*. Documentation and Users Manual. Civil and Environmental Engineering Dept., Tufts University, Medford, MA.
- Daly, C., Halbleib, M., Smith, J.I., Gibson, W.P., Doggett, M.K., Taylor, G.H., Curtiss, J., Pasteris, P.P., 2008. Physiographically sensitive mapping of climatological temperature and precipitation across the conterminous United States. *Int. J. Climatol.* 28 (15), 2031–2064. <https://doi.org/10.1002/joc.1688>.
- Donnelly, J.P., King, S.L., Silverman, N.L., Collins, D.P., Carrera-Gonzalez, E.M., Lafón-Terrazas, A., Moore, J.N., 2020. Climate and human water use diminish wetland networks supporting continental waterbird migration. *Glob. Change Biol.* 26 (4), 2042–2059. <https://doi.org/10.1111/gcb.15010>.
- Dunn, D.. Salt Lake Mass Balance Model Data Collection. HydroShare. <http://www.hydroshare.org/resource/267e083484a74866927d91bdef60f8d6>.
- Dunn, D., Crookston, B.M., Phillips, C., Dutta, S., Neilson, B., 2025. Seasonal water and salt cycling in the Great Salt Lake after opening the new causeway breach. *J. Hydrol. Reg. Stud.* 59, 102332. <https://doi.org/10.1016/j.ejrh.2025.102332>.
- Dutta, S., Crookston, B.M., Dunn, D., Larsen, E., Talukdar, M.I.H., 2024. *Predicting temporal evolution of salt mass within the Great Salt Lake under adaptive berm management and changing lake conditions* (Report No. 4747). Utah Water Research Lab, Utah State University.
- ECONorthwest, Martin and Nicholson Environmental Consultants, 2019. Assessment of potential costs of declining water levels in Great Salt Lake. Retrieved from <https://documents.deq.utah.gov/water-quality/standards-technical-services/great-salt-lake-advisory-council/activities/DWQ-2019-012913.pdf>.
- Ford, D.E., Johnson, L.S., 1986. An assessment of reservoir mixing processes. Technical report E-86-7. Ford, Thornton, Norton and Associates, Ltd. (for the U.S. Army Engineer Waterways Experiment Station, Vicksburg, MS. Retrieved from <https://usace.contentdm.oclc.org/digital/collection/p266001coll1/id/2728/>
- Great Salt Lake Strike Team, 2023. Great Salt Lake policy assessment: a synthesized resource document for the 2023 general legislative session 2023. Retrieved from <https://gardner.utah.edu/wp-content/uploads/GSL-Assessment-Feb2023.pdf?x71849>.
- GSLIM. (2019). [Evaluation]. Jacobs Engineering. Retrieved from <https://documents.deq.utah.gov/water-quality/standards-technical-services/great-salt-lake-advisory-council/DWQ-2022-028692.pdf>.
- Gwynn, W., Sturm, P., 1987. Effects of breaching the GSL causeway, Great Salt Lake, Utah—Physical and chemical changes August 1, 1984–July, 1986. Utah Geological and Mineral Survey. Retrieved from https://ugspub.nr.utah.gov/publications/water_resources_bulletins/WRB-25.pdf.

- Hassani, A., Azapagic, A., D'Odorico, P., Keshmiri, A., Shokri, N., 2020. Desiccation crisis of saline lakes: a new decision-support framework for building resilience to climate change. *Sci. Total Environ.* 703, 134718. <https://doi.org/10.1016/j.scitotenv.2019.134718>.
- Hoffman, J.D., 2001. *Numerical Methods for Engineers and Scientists*, Second ed. Marcel Dekker, Inc. Retrieved from (http://freeit.free.fr/Finite%20Element/Hoffman,_Numerical_Methods_for_Engineers&Scientists,2001.pdf).
- Holley, E., R, Waddell, K.M., 1976. Stratified Flow in Great Salt Lake Culvert. *J. ASCE Hydraul. Div.* 17. <https://doi.org/10.1061/JYCEAJ.000459>.
- Horsburgh, J.S., Jones, A.S., Black, S.S., Hodson, T.O., 2022. USGS data retrieval python package usage examples. HydroShare. (<http://www.hydroshare.org/resource/c97c32ecf59b4df90ef013030c54264>).
- Huntington, J., Hegewisch, K., Daudert, B., Morton, C., Abatzoglou, J., McEvoy, D., Erickson, T., 2017. Climate engine: cloud computing of climate and remote sensing data for advanced natural resource monitoring and process understanding. *Bull. Am. Meteorol. Soc.* (<http://journals.ametsoc.org/doi/abs/10.1175/BAMS-D-15-00324.1>).
- Jagniecki, E., Rupke, A., Kirby, S., Inkenbrandt, P.I., 2021. Salt crust, brine, and marginal groundwater of Great Salt Lake's north arm (2019 To 2021). Utah Geological Survey. <https://doi.org/10.34191/R1-283>.
- Jewell, P.W., 2021. Historic low stand of Great Salt Lake, Utah: I: mass balance model and origin of the deep brine layer. *SN Appl. Sci.* 3 (8), 757. <https://doi.org/10.1007/s42452-021-04691-5>.
- Larsen, E., 2024. Rapid prediction of Buoyancy-Driven exchange flows at the Great Salt Lake: ML 832 models and a 1D shallow water approach. Thesis. Utah State University. 833. (<https://digitalcommons.usu.edu/etd2023/319/>).
- Lindsay, et al., 2019. Effects of salinity on microbialite-associated production in Great Salt Lake Utah. *Ecol. Soc. Am.* 100 (3). <https://doi.org/10.1002/ecy.2611>.
- Loving, B.L., Waddell, K.M., Miller, C.W., Utah Division Of Forestry, F.A.S.L. & Tooele County. (2000). Water and salt balance of Great Salt Lake, Utah, and simulation of water and salt movement through the causeway, -98. [Salt Lake City, Utah: U.S. Dept. of the Interior, U.S. Geological Survey; Denver, CO: Branch of Information Services distributor] [Image]. Retrieved from the Library of Congress, (<https://www.loc.gov/item/2001337137/>).
- Lukens, E., Turney, E.K., Null, S., Neilson, B., 2024. Measurement and infrastructure gap analysis in utah's Great Salt Lake basin. HydroShare. <https://doi.org/10.4211/hs.8bf055dbe78b46d184cc7a4bb53931c7>.
- Marden, B., Brown, P., Bosteels, T., 2020. Great Salt Lake artemia: ecosystem functions and services with a global reach. In: Baxter, In.B.K., Butler, J.K. (Eds.), *Great Salt Lake Biology*. Springer International Publishing, pp. 175–237. https://doi.org/10.1007/978-3-030-40352-2_7.
- McIlwain, H.E., Arias, M.C., McDonnell, M.C., Seawolf, S.M., Rumsey, C.A., 2023. Vertical water-quality profiles collected at Great Salt Lake monitoring sites, utah, 1995–2022. In: U.S. Geological Survey data release. U.S. Geological Survey. <https://doi.org/10.5066/P9J6A07X>.
- Merck, M.F., Tarboton, D.G., 2023. The salinity of the Great Salt Lake and its deep brine layer. *Water* 15 (8), 1488. <https://doi.org/10.3390/w15081488>.
- Mohammed, I.N., Tarboton, D.G., 2006. *Modeling the Great Salt Lake*. Utah State University.
- Mohammed, I.N., Tarboton, D.G., 2012. An examination of the sensitivity of the Great Salt Lake to changes in inputs: Great Salt Lake Sensitivity Index. *Water Resour. Res.* 48 (11). <https://doi.org/10.1029/2012WR011908>.
- Naftz, D.L., 2017. Inputs and internal cycling of nitrogen to a causeway influenced, hypersaline lake, Great Salt Lake, utah, USA. *Aquat. Geochem.* 23 (3), 199–216. <https://doi.org/10.1007/s10498-017-9318-6>.
- Naftz, D.L., Carling, G.T., Angeroth, C., Freeman, M., Rowland, R., Pazmiño, E., 2014. Density-Stratified flow events in Great Salt Lake, Utah, USA: implications for Mercury and salinity cycling. *Aquat. Geochem.* 20 (6), 547–571. <https://doi.org/10.1007/s10498-014-9237-8>.
- Naftz, D.L., Miller, B.J., Jones, B.F., Reed Green, W., 2011. An equation of state for hypersaline water in Great Salt Lake, utah, USA. *Aquat. Geochem.* 17 (6), 809–820. <https://doi.org/10.1007/s10498-011-9138-z>.
- Null, S.E., Wurtzbaugh, W.A., 2020. Water development, consumptive water uses, and Great Salt Lake. In: Baxter, B., Butler, J. (Eds.), *Great Salt Lake Biology*. Springer, Cham. <https://doi.org/10.1007/978-3-030-40352-2>.
- Oberg, K., Morlock, S., Caldwell, W., 2005. Quality assurance plan for discharge measurements using acoustic Doppler current profilers. U.S. Geologic Survey; Scientific Investigations Report 2005-5183. Retrieved from (https://pubs.usgs.gov/sir/2005/5183/SIR_2005-5183.pdf).
- Otto, S.P., 2018. Adaptation, speciation and extinction in the anthropocene. *Proc. R. Soc. B Biol. Sci.* 285 (1891), 2018–2047. <https://doi.org/10.1098/rspb.2018.2047>.
- Perry, K.D., Crossman, E.T., Hoch, S.W., 2019. Results of the Great Salt Lake dust plume study (2016–2018) (Tech. Rep.). Department of Atmospheric Sciences, University of Utah. Retrieved from (https://d1bbnjcm4wtr1.cloudfront.net/wp-content/uploads/2019/12/10101816/GSL_Dust_Plumes_Final_Report_Complete_Document.pdf).
- Rasmussen, M., Dutta, S., Neilson, B.T., Crookston, B.M., 2021. CFD model of the density-driven bidirectional flows through the west crack breach in the Great Salt Lake causeway. *Water* 13 (17), 2423.
- Root, J.C., 2023. Half-meter topo bathymetric elevation model and elevation-area-volume tables for Great Salt Lake, utah, 2002–2016. U.S. Geological Survey data release. <https://doi.org/10.5066/P9DGG75W>.
- Sundaram, T.R., Rehm, R.G., 1973. The seasonal thermal structure of deep temperate lakes. *Tellus* 25 (2), 157–168. <https://doi.org/10.1111/j.2153-3490.1973.tb01602.x>.
- Tarboton, D., 2024. Collection of Great Salt Lake Data. HydroShare. (<http://www.hydroshare.org/resource/b6c4fcad40c64c4cb4dd7d4a25d0db6e>).
- U.S. Geological Survey. (2023). National Water Information System data available on the World Wide Web (USGS Water Data for the Nation). U.S. Geological Survey. Retrieved October 10, 2023, from (<http://waterdata.usgs.gov/nwis/2023>).
- U.S. Geological Survey. (2006). Collection of water samples (Version 2.0) [Chapter A4, National Field Manual for the Collection of Water-Quality Data, Book 9, Techniques of Water-Resources Investigations]. U.S. Department of the Interior. [\(https://pubs.usgs.gov/twri/twri9a4/twri9a4_Chap4_v2.pdf\)](https://pubs.usgs.gov/twri/twri9a4/twri9a4_Chap4_v2.pdf) (pubs.usgs.gov).
- University of Utah. (2024). Hatut Station Metadata Page. MESOWEST. Retrieved June 7, 2024, from (https://mesowest.utah.edu/cgi-bin/droman/station_total.cgi?stn=HATUT) and unit=0.
- US Geological Survey. (2019). *USGS Techniques and Methods Specific Conductance* (National Field Manual for the Collection of Water-Quality Data, pp. 9-A6.3, 12) [Techniques and Methods].
- Utah Department of Natural Resources, 2022. *Great Salt Lake water budget overview*. Utah Department of Natural Resources: Water Resources, Salt Lake City, Utah.
- Utah Department of Water Quality, 2022. Union pacific railroad Great Salt Lake permanent east culvert closure and bridge construction project. Retrieved from (<https://documents.deq.utah.gov/water-quality/facilities/401-wq-cert/DWQ-2022-001884.pdf>).
- Utah Division of Forestry, Fire and State Lands, 2013. Final Great Salt Lake comprehensive management plan and record of decision. Utah Division of Forestry, Fire and State Lands, Salt Lake City, UT (accessed on January 6, 2023).
- Utah Geological Survey, 2020. Great Salt Lake brine chemistry database: online. (https://geology.utah.gov/docs/xls/GSL_brine_chem_db.xlsx).
- Utah State University (2024). Surface Weather and Climate Observations. Utah Climate Center. Retrieved January 24, 2024, (<https://climate.usu.edu/swco>).
- Waddell, K.M., Fields, F.K., 1977. Model for Evaluating the Effects of Dikes on the Water and Salt Balance of Great Salt Lake Utah. Retrieved from (https://ugspub.nr.utah.gov/publications/water_resources_bulletins/WRB-21.pdf).
- Wang, S.-Y., Gillies, R.R., Jin, J., Hippis, L.E., 2010. Coherence between the Great Salt Lake level and the pacific Quasi-Decadal oscillation. *J. Clim.* 23 (8), 2161–2177. <https://doi.org/10.1175/2009JCLI2979.1>.
- White, J.S., Null, S.E., Tarboton, D.G., 2015. How do changes to the railroad causeway in Utah's Great Salt Lake affect water and salt flow? *PLOS ONE* 10 (12), e0144111. <https://doi.org/10.1371/journal.pone.0144111>.
- Williams, W.D., 1996. The largest, highest and lowest lakes of the world: saline lakes. *SIL Proc.* 19222010 26 (1), 61–79. <https://doi.org/10.1080/03680770.1995.11900693>.
- Williams, A.P., Cook, E.R., Smerdon, J.E., Cook, B.I., Abatzoglou, J.T., Bolles, K., Baek, S.H., Badger, A.M., Livneh, B., 2020. Large contribution from anthropogenic warming to an emerging north American megadrought. *Science* 368 (6488), 314–318. <https://doi.org/10.1126/science.aaz9600>.
- Wold, S.R., Thomas, B.E., and Waddell, K.M. (1996). Water and salt balance of Great Salt Lake, Utah, and simulation of water and salt movement through the causeway (Open-File Report 95-428; p. 76). Retrieved from (<https://pubs.usgs.gov/of/1995/0428/report.pdf>).

- Wurtsbaugh, W.A. (2014). Management of the Great Salt Lake Ecosystem: Water, Economic Values and Competing Interests. Watershed Sciences Faculty Publications, Paper 594. Retrieved from (https://digitalcommons.usu.edu/wats_facpub/594).
- Wurtsbaugh, W.A., and Jones, E.F. (2012). The Great Salt Lake's Deep Brine Layer and Its Importance for Mercury Bioaccumulation in Brine Shrimp (*Artemia franciscana*). Watershed Sciences Faculty Publications, Paper 551. Retrieved from (https://digitalcommons.usu.edu/wats_facpub/551).
- Wurtsbaugh, W.A., Miller, C., Null, S.E., DeRose, R.J., Wilcock, P., Hahnberger, M., Howe, F., Moore, J., 2017. Decline of the world's saline lakes. Nat. Geosci. 10 (11), 816–821. <https://doi.org/10.1038/ngeo3052>.
- Yang, S., Johnson, W.P., Black, F.J., Rowland, R., Rumsey, C., Piskadlo, A., 2020. Response of density stratification, aquatic chemistry, and methylmercury to engineered and hydrologic forcings in an endorheic lake (Great Salt Lake, U.S.A.). Limnol. Oceanogr. 65 (5), 915–926. <https://doi.org/10.1002/limo.11358>.
- Zamora, H.A., Inkenbrandt, P., 2024. Estimate of Groundwater Flow and Salinity Contribution to Great Salt Lake Using Groundwater Levels and Spatial Analysis. Utah Geological Association Publication.